Universität Bremen

✉ Universität Bremen **I MARUM I** 28359 Bremen

Dr.
Thomas Westerhold
Research Scientist

Leobener Strasse 8
MARUM building, Room 0220
28359 Bremen – Germany

Telefon   +49 421 218 – 65672
E-Mail   twesterhold@marum.de
www   www.marum.de

To the Editors of

Climate of the Past

.

23/January/2018

Dear Yves Godderis (Editor),

Please accept our submission of the revised manuscript entitled "Synchronizing early Eocene deep-sea and continental records – cyclostratigraphic age models for the Bighorn Basin Coring Project drill cores" for consideration by *Climate of the Past*.

Thank you very much for your editorial work and suggestions. We greatly appreciate your effort and would like to thank the two referees for their critical reviews, all of which improved the manuscript. Comments and constructive criticism encouraged us to carefully revise the manuscript.

Detailed answers to the comments of the referees were already posted on the *Climate of the Past Discussions* web page. Here we address all issues raised by the referees point-by-point to improve the manuscript.

We hope that the revised manuscript now meets the requirements to be published in *Climate of the Past*.

Kind Regards,
Thomas Westerhold, Ursula Röhl, Roy Wilkens, Philip Gingerich, Will Clyde, Scott Wing, Gabe Bowen, Mary Kraus

The original referees' comments are indicated by italics, our response is marked by red letter.

Referee #1

MAJOR POINTS

Title*: Looking at the ms, one may ask why new is included. Are these new cyclostratigraphic age models for the BBCP cores, but then what are the old cyclostratigraphic age models from the project. Moreover, these age models are also not particularly new when compared with the existing age models based on outcrops, as these are largely identical.*

We change the title of the manuscript to "Synchronizing early Eocene deep-sea and continental records – cyclostratigraphic age models for the Bighorn Basin Coring Project drill cores".

MTM spectra 1*. The MTM spectra might be somewhat problematical as the null- spectrum and confidence limits do not follow the shape of the spectrum very well. Is this a problem of using the "wrong" model for calculating the null-spectrum (as in Vaughan et al., 2011)? Is it as such logical that the power of all thicknesses between ~ 2 and ~ 20 m plot above the 99% CL? This band contains the dominant 3.5 and 8 m cycles, but constant power above 99% for such a broad frequency is not very logical.*
In this respect, the authors should preferably not use the Mann and Lees (1996; ML96) robust red noise approach that is in SSA-MTM tookit, as it has a tendency to artificially create low frequency cycles (as documented in Meyers, 2012; example in his Figure 2D illustrates that there is a 90% chance of getting false long period cycles from noise). If they want to use the ML96 approach, they should use the one in Astrochron, which fixes this 'edge-effect' problem.

All MTM spectra have been replaced by mtmML96 spectra using the Astrochron software package. The methods section was modified accordingly.

The MTM spectra often show a bewildering numbering of peaks in the frequency band that is of primary interest for the paper. This large number of peaks likely stems from the very long and high-resolution character of the records, but it might be preferable to attempt reducing the number of spectral peaks in this band, as less peaks / resolution imply greater stability of peak position, and is more easy to interpret.

We agree. Due to the high resolution of the expanded records the spectra show lots of details. Because the spectra have been calculated for the entire length of each record, changes in sedimentation rates will produce several closely spaced peaks. To be able to identify changes in sedimentation rates the evolutive spectra were calculated. For the extraction of cycles by filtering of the signal we applied a 30% bandwidth to compensate for these variations in cycle thickness as described in the manuscript.

MTM spectra 2*. The dramatic reduction of power at very low frequencies in their MTM spectra is due to the data detrending. My concern is that the frequencies they are interested in are up against this detrended region of the spectrum. So if they want to do this detrending, they should also show power spectra without the trends removed, so one can better evaluate the nature of the peaks (if they are real or a consequence of detrending).*

We now provide MTM spectra using the mtmML96 Astrochron routine for all data. The detrending removed cycles longer than 10m, not relevant for the study.

Half-precession*. The authors constantly use the term half precession cycle for their 3.5 m cyclicity while their precession related cycles are often more than twice as thick. This problem was also encountered by Abdul-Aziz et al. (2008), when studying the Polecat Bench and Red Butte sections;*

they concluded that this cycle, which is related to prominent individual paleosols, does not represent half (or semi-) precession, but has a period that is significantly shorter and closer to that of the Heinrich events of the last 100.000 year. This was confirmed by the results of bandpass filtering, and the same is the true for the results of the filtering in the present ms (see their Figure 5 where more than two cycles fit into one precession-related cycle). Hence, the authors should use sub-precession or millennial-scale rather than half-precession.

We have corrected this in the resubmitted version of the manuscript. However, it is not important for the cyclostratigraphy which is based on the recognition of the precession cycle only.

Precession minimum *(l. 24, p. 9). The authors mention that the PETM onset was in a precession minimum, but it is not clear where that comes from (they refer to see above). Do they mean the Fe-minimum between their cycle 1 and -1? But where is the phase relation with precession based on, or it this a mistake? It is also not perfectly clear to me how that might explain the 4-kyr discrepancy in addition of the one precession cycle misfit, also because discrepancies of 4-kyr are within the uncertainty of all the age models.*

We have clarified this in the revised version of the manuscript. The following was added after (page 7, line 19): "… also assume that the onset of the PETM is located in the minimum between cycle -1 and 1": *Regarding the phase relationship, whether paleosols correspond to precession minima or maxima (Abels et al., 2013) is unknown and not relevant for establishing a cyclostratigraphy based on cycle counting itself. For simplicity we assume that paleosols correspond to more negative bulk carbonate carbon isotope values in more clay rich layers in the deep-sea records (higher Fe XRF intensities, Zachos et al., 2010; Littler et al., 2014; Zeebe et al. ,2017). Thus, the onset of the PETM was set into a precession minimum in the PCB cyclostratigraphy model.*

Comparison between cyclostratigraphic and Helium-based age models. *(l.10-28, p.10). This discussion is becoming a bit semantic and potentially far-fetched, going into much detail, which may not all be that relevant to explain the observed major offset of 40-kyr for the initial rapid recovery of the CIE. Also, the average duration of a precession cycle remains an average and longer precession periods are generally found in intervals with high eccentricity (maxima) and shorter cycles during eccentricity minima (as the different cycles are differently modulated), so this plays a role as well. However, again the difference might be either too small to explain the offset or will only (slightly) enhance it. A relevant question to ask is whether the Helium isotope ratio is not affected (or not) by the enhanced volcanic activity at that time as the East Greenland flood basalts may have formed at the same time (see Wotzlaw et al.).*

We thank the referee for this comment. A sentence is added mentioning the Wotzlaw et al. 2012 study. We think discussing or showing the effects of your new age model compared to the Helium age model is important and could be basis for further research, but we refrain from going into too much detail because this is not the scope of our study.

Almost. *A very interesting and also intriguing aspect is the potential causal connection between Biohorizon B in the Bighorn Basin and the calcareous nannofossil events of the same age in the marine realm, intriguing especially as the proxies in the marine record do not indicate that something dramatic is happening. However, the authors use the curious wording almost when comparing the continental faunal turnover with the marine events. But almost is not of the same age, so what is exactly the difference and how does almost the same age translate to potentially having the same origin. In Figure 8, the age difference between the two events is ~ 40-kyr, but what are the uncertainties in the respective age models and in the position and thus age of the respective bio-events? The uncertainty in the position of Biohorizon B might be quite large compared with that in the marine record, so do these uncertainties overlap? The reason to develop high-resolution astrochronologic age models is meant to increase the temporal resolution and solve possible*

temporal relationships and chicken-and- egg problems. So what does this almost imply in this case? This should be made more clear in the ms.

This section is rewritten now (as outlined in the discussion phase), the position has been revised and clarified including a proper error discussion and updated Figure 8.

MINOR POINTS

Cycle 0. *Why is there no cycle 0 in the numbering of the cycles in the PCB cores*

Why should there be a cycle 0? It is not clear what the referee is pointing at. The onset of the PETM was chosen as the zero line (Table 1 of the ms), in-between precession cycle -1 (before onset PETM) and 1 (after onset PETM).

405-kyr minimum *(p.7, l. 14). Is this also not part of a very long 2.0 Myr eccentricity cycle, see Lourens et al., (2005) and Meyers (2015)? Please check what you mean exactly.*

It is correct as written. The cycles occur in a 405-kyr minimum, a time of low amplitude modulation of the precession cycle by eccentricity.

3.2 Time series analysis of BBCP drill cores. *The first paragraph before 3.2.1 belongs to the Material & Methods section rather than to Results.*

We would like to keep this section where it is because the time series analysis and thus age model development should ideally be in one chapter.

Referee #2

MAJOR POINTS

1) The definition of the end of CIE-PETM in the Polecat Bench δ13C record

Duration estimates of the PETM and comparison with previous studies depend tightly on how the stratigraphic extent of CIE is defined. While it is easier to define the onset of CIE at both realms, the definition of its end is more problematic, especially in the continental δ13C record.

In the present form of the ms, it is not clear how the authors (or may be by referring to previous papers) set the end of CIE in the δ13C terrestrial record. Based on their figure 5, I can place it appropriately at 60 mcd depth, and largely at 55 mcd depth. This implies respectively 7.5 to 8 precession cycles, yielding respective durations of 157.5 and 168 kyr (21 kyr mean precession period). These durations are close to the 171 kyr estimate inferred from deep-sea records (Röhl et al., 2007).

Definitions for the different phases of the PETM in the deep-sea and the terrestrial realm are given in Zachos et al. 2005, Röhl et al. 2007, Murphy et al. 2010 (all three deep-sea) and Bowen et al. 2015 (Polecat Bench record). We think it is not very helpful to reiterate the definitions again in the manuscript, citation of those seems to be the best way.

The CIE in the BBCP Polecat Bench drill core has been defined and discussed in Bowen et al. 2015. Assuming, as proposed by the referee above, that the PETM CIE lasted from the onset (118.70 mcd – Bowen et al. 2015) and 55 to 60 mcd (~58.20 mcd) at PCB results in a duration (applying the Table 1 age model) of 157 kyr.

But as written on page 9, line 14: "At the Walvis Ridge ODP sites, the top of the clay layer coincides with the top of the initial rapid recovery of the CIE (Recovery phase I in Murphy et al., 2010). To correlate deep-sea and terrestrial records, the onset and the top of the initial rapid recovery of the CIE are commonly used (McInerney and Wing, 2011)". It is important to know, as written in McInerney and Wing, 2011, that the top of the initial rapid recovery (phase I in Röhl et al. 2007) of the CIE is NOT the top of the subsequent gradual recovery (phase II in Röhl et al. 2007) as assumed by

the referee. This matter is complex and can be confusing, but using the definitions as given in Röhl et al. 2007, and more deeply discussed by Murphy et al. 2010, the results of this manuscript clearly show that the duration in the deep-sea is about one precession cycle shorter that in the terrestrial Polecat Bench section.

In all figures dealing with CIE's correlation between terrestrial and deep-sea records (Figures 7, S12 and S13), the onset of CIE is clearly shown at the abrupt negative δ13C shift, whereas the end of CIE is not obvious neither at ODP sites nor in PCB terrestrial record. It's even sometimes confused when reading the cyclostratigraphic interpretation against the proposed age model, and what is said in the text. For instance, in figure 7, the duration of the entire CIE is assessed at about 180 kyr (120 kyr for the clay layer indicated by the brown rectangle plus 59 kyr till the end of CIE shown by light blue rectangle). In the text, the authors discuss a longer duration of 200 kyr..
Again, considering a very likely end of CIE in the terrestrial δ13C data at the top (maximum) of precession cycle no. 8 (Fig. 7), a duration of 168 ky (21 kyr x 8 cycles) could be inferred..

We admit that the definition of phases needs clarification, which is now done in the discussion by adding 17 lines of text to the discussion.

A focus was also given on the duration of clay-layer interval. The clay layer is characteristic of deep-sea environment. What is the degree of reliability of correlation between terrestrial and deep- sea (using δ13C) data that led to the projection of equivalent clay-layer interval into the terrestrial records? Note that this correlation is crucial for the assessment of duration of the clay layer. Could the authors add uncertainties on their stratigraphic correlation?

This was discussed on page 9, lines 16 to 34 of the submitted initial manuscript and is still part of the revised manuscript. The onset of the PETM is clearly correlated by the dramatic shift in carbon isotopes. In marine sediments this is the base of the clay layer. The top of the clay layer, in marine sediments of Walvis Ridge, coincides with the top of the initial rapid recovery of the CIE (Recovery phase I in Murphy et al., 2010). The relatively fast rate of carbon exchange between atmosphere and surface (10's of years) and deep (100's of years) ocean reservoirs requires that the rapid recovery in marine and terrestrial records should be recorded at almost the same time. Using the Röhl et al. 2007 age model as time lag of 25 kyr is apparent between the PCB record and marine data. Assuming that this rapid shift should be nearly synchronous, as written in the ms, we concluded that 25 kyr or about one precession cycle could be missing in the marine records due to the severe dissolution at the onset of the PETM.

In summary, the authors should state clearly in the manuscript how they define the stratigraphic extent of the entire CIE (especially its end) and the projected clay-layer into the terrestrial records, and accordingly they could compare duration estimates between the two realms.

We have add 17 lines of text to the discussion dealing with this issue.

2) Comparison with previous age models
In the outcrops (Bighorn Basin) in the Polecat Bench section, Abdul-Aziz et al. (2008) arrived to a duration of 157 kyr for the entire CIE-PETM.
Westerhold and co-authors cited Abdul-Aziz et al.'s (2008) study, but they did not explain the 157 kyr shorter duration compared to their longer duration of 200 kyr obtained from Polecat Bench drill cores. Given both studies are based on precession cycle counting from the same basin (and the same Polecat Bench site), I strongly recommend that the authors explicitly discuss the source of such significant difference. Although the authors evoked promptly this difference (Page 7, lines 21-23), but it is still ambiguous how they found a longer duration with regard to a shorter duration provided by Abdul-Aziz et al. (2008) (see also 'Comment 1' above).
Note that Abdul-Aziz et al.'s (2008) duration estimate (i.e., 157 kyr) is close to the 171 kyr duration of Röhl et al. (2007) inferred from deep-sea records.

"The main body of the CIE spans ~5.5 precession cycles, or ~115 k.y., and the recovery tail of the CIE spans 2 precession cycles, or ~42 k.y." (157 kyr) – Abdul-Aziz et al. 2008.

Again, as already discussed above, the issue here is the definition of different phases of the PETM. The duration for the main body of the PETM, as written in the ms, is almost identical to Abdul-Aziz et al. 2008. The recovery phases of the PETM CIE have been defined in deep-sea records (Zachos et al. 2005, Röhl et al. 2007). Rapid recovery from the CIE should be nearly synchronous in both records. But it is rather difficult to identify the end of the recovery phase (the inflection point G mentioned in the revised manuscript) in other records (including the PCB records) than ODP 690. In Abdul-Aziz et al. 2008 the recovery is from ~63 to ~77m, a distance of 14 m (their Figure 3) containing two precession cycles. The new higher resolution data for the PETM CIE from Bowen et al. 2014 show that the recovery starts (note that the depth in the core is from top down, in the outcrop from bottom up) at 75m and ends at 55m, a distance of 20m. We do not want to discuss here which definition at Polecat Bench is correct, but rather point to the fact that is comes down to this definition to find out the duration of the PETM at Polecat Bench. Concerning the marine records, and applying the definitions given in Zachos et al. 2005 and Röhl et al 2007, the duration of the PETM determined in our manuscript remains at 196 kyr, roughly 200 kyr.

In a revised manuscript, we have clarified this by pointing to the rather difficult identification of the inflection point G in the Polecat Bench records.

3) Amplitude modulation (AM) of the precession by the eccentricity
The authors outlined 'AM of the precession by the eccentricity' in the text body and they also pointed it out in the abstract and conclusions, however, there is no statistical test (or even an attempt by visual inspection) to show or retrieve such modulation. If the authors would still retain this result, then they should demonstrate it, at least at the short eccentricity band.
The authors stated (Page 7, lines 8 and 9) : "The filter of the precession cycles of ~8.2 m in both data show modulations that are consistent with eccentricity". Filtering is not sufficient to draw such conclusion. Here a Hilbert transform is required to extract such AM envelopes...

We added a Hilbert transform of the data to the revised figure 5.

4) Half-precession
Precession vs half-precession ratio is not consistent with the selected bandwidths used for filtering (see for e.g., Fig. 5). Visual inspection in figure 5 indicates that several precession cycles do not match two 'half-precession' cycles, making the hypothesis of 'half-precession' implausible. Also, if the precession central wavelength is 8.2 m, then 'half-precession' central wavelength should be around 4 m (not 3.45 m).
Can the authors resolve this mismatch, by changing the bandwidth for example, or abandon the hypothesis of 'half-precession'.
In addition, the authors stated (Page 5, Lines 28-29) "The two longer cycles around 8 and 3.5 m have been interpreted as precession and half precession cycles also present in Plio-Pleistocene successions (see Abdul-Aziz et al., 2008)."
Abdul-Aziz et al. (2008) did not interpret the 3.5 m cycles as half-precession. Instead, they interpreted them as sub-Milankovitch (or millennial). They even stated in their paper « However, the exact origin of sub-Milankovitch cycles remains enigmatic. ». Sub-Milankovitch (or millennial-scale) cycles do not imply half-precession cycles...

This was mentioned by referee #1 as well. We have corrected this in a resubmitted version of the manuscript. It is not important for the cyclostratigraphy which is based on the recognition of the precession cycle only.

5) Significance of changes in sediment a* color reflectance and Fe content in terrestrial records

Although the authors evoked very promptly the potential significance of XRF iron intensity in terrestrial sediments by referring to previous studies (Abels et al., 2012), [and this topic is beyond the scope of the present study], I suggest that the authors develope a little bit the significance of such proxies in terms of climate change (astronomically forced climate). Orbitally driven fluctuations in Fe content in deep-sea sedimentary records have generally (and extensively) been attributed to the relative contribution from carbonate deposition versus detrital-clay inputs. However, the origin of cyclic change in Fe content in terrestrial environments is not well addressed in the literature...

It is not the scope of the manuscript to discuss and explore the nature of Fe variations and its direct links to climate change. This requires detailed geochemical analysis, as already done in Kraus et al. 2015 (Palaeogeography, Palaeoclimatology, Palaeoecology 435 (2015) 177–192; http://dx.doi.org/10.1016/j.palaeo.2015.06.021) at Polecat Bench, on two PCB drill cores. Our focus is on using the apparent cyclicity for age model construction.

The XRF core scanning method applied provides semi-quantitative information of bulk iron concentrations. It does not distinguish oxidation states of Iron necessary to address imprints of climate change on the sediment Fe composition as done in Kraus et al. 2015. Looking at Fe only it is not possible to speculate about humidity, this can be done by combining elemental information into ,e.g., the chemical index of alteration (CIA) done for Polecat Bench by Kraus and Riggins (2007). We are currently working on exactly this topic towards an additional manuscript dealing with XRF core scanning data from the BBCP drill cores. We would like not to include the discussion of the potential significance of XRF iron intensity in the BBCP records because this will be focus of a subsequent manuscript following the our here presented age model study.

Minor points

Page 1, Lines 19 to 20:
"A consistent stratigraphic framework is required to understand the effect of major climate perturbations of the geological past on both marine and terrestrial ecosystems."
Should better be:
"A consistent chronostratigraphic framework is required to understand the effect of major paleoclimate perturbations on both marine and terrestrial ecosystems."
corrected

Page 1, Line 25:
"Bighorn Basin Drilling Project (BBCP, Wyoming, USA)"
Please change into: "Bighorn Basin Coring Project (BBCP, Wyoming, USA)"
corrected

Page 1, Lines 29 to 30 :
"The duration of the PETM is estimated at ~200 kyr for the CIE and ~120 kyr for the pelagic clay layer."
Should better be: The duration of the PETM is estimated at ~200 kyr for the CIE and ~120 kyr for the associated pelagic clay layer.
corrected

Page 2, Lines 7 & 8:
"Both have been studied in great detail in both in deep-sea sedimentary and terrestrial successions (Zachos et al., 2005; Abels et al., 2016)."
Into: Both have been studied in great detail in deep-sea and terrestrial sedimentary successions (e.g., Zachos et al., 2005; Abels et al., 2016)."
corrected

Page 2, Lines 10, 11 & 12:

"The hyperthermal events in outcrops and ocean drill cores can be identified by the characteristic negative carbon isotope excursions (CIEs), although these differ in magnitude (McInerney and Wing, 2011; Bowen, 2013)."
Magnitude of PETM CIE should also refer to Sluijs and Dickens (2012) (Global Biogeochemical Cycles 26, GB4005).
added

Page 2, Lines 12 & 13:
"The CIEs are interpreted as massive inputs of δ13C-depleted carbon to the exogenic carbon pool (see Dickens et al., 2011 for discussion)."
Into: "The CIEs are interpreted as due to massive inputs of δ13C-depleted carbon to the exogenic carbon pool (see Dickens et al., 2011 for discussion)."
corrected

Page 2, Line 21:
"... understanding the future of climate on Earth ..."
into: "... understanding Earth's future climate ..."
corrected

Page 2, Lines 27 & 28:
"Deep-sea records have a much lower sedimentation rate (cm/kyr) compared to the terrestrial records (m/kyr), but have been deposited continuously."
Into: Deep-sea records have much lower sedimentation rates in the order of cm/kyr compared to the terrestrial records having sedimentation rates in the order of m/kyr...
corrected

Page 2, Lines 28 to 30:
"Sedimentation at the terrestrial successions very likely was more dynamic due to the different types of deposition (see Bowen et al., 2015)."
Into: "Sedimentation in terrestrial environments was very likely more dynamic due to the different types of deposition (see Bowen et al., 2015). "
corrected

Page 2, Lines 30 & 31:
"To interpret rates of changes and processes before, during and after the events a detailed age model is required."
Into: "To interpret rates of changes of geological processes before, during and after the events a detailed age model is required."
corrected

Page 2, Lines 34 to 36:
"Estimates for the duration of the PETM from deep-sea records are complicated by severe carbonate dissolution, which forms a clay-rich layer at the onset of the event (Röhl et al., 2007)."
Into: "Cyclostratigraphic estimates of the duration of the PETM from deep-sea records are hampered by the lack of carbonate-rich sequences, which are characacterized on sites nearby the paleo-CCD with a clay- rich layer at the onset of the event (Röhl et al., 2007), resulting from severe carbonate dissolution (Zachos et al., 2005)."
corrected

Page 3, Lines 11 to 15 :
"The purpose of this report is to establish high-resolution age models for the BBCP drill cores based on cyclostratigraphy and integrate existing age models from outcrops. Second, these new BBCP drill

cores age models will be combined with deep-sea records to synchronize and improve the available astronomical age model for the PETM and Elmo interval."
Remove "Second" or change into: "The main purpose of this report is to establish high-resolution age models for the BBCP drill cores based on cyclostratigraphy and integrate existing age models from outcrops. Second, these new BBCP drill cores age models will be combined with deep-sea records to synchronize and improve the available astronomical age model for the PETM and Elmo interval."
corrected

Page 3, Line 31:
"... the BSN and GMH and PCB sites." Into:
"... the BSN, GMH and PCB sites."
corrected

Page 4, Lines 12 to 26:
All this paragraph deals with isotope data acquisition, which were already presented in Bowen et al. (2015). Thus, such paragraph should be removed or shortened or moved to the supplementary materials.
corrected, we removed this particular methods section, now citing Bowen et al. (2015).

Page 5, Line 15:
"3.2 Timeseries analysis of BBCP drillcores", please add a hyphen to 'Time-series' and to 'drill-cores' (or a space 'drill core')
corrected

Page 8 (Line 34) and page 9 (Line 1):
"During the PETM, massive dissolution of carbonates in the deep sea truncated the record (Zachos et al., 2005), complicating the age model constructions."
Into: "During the PETM, massive dissolution of carbonates in the deep sea truncated the cyclostratigraphic record (Zachos et al., 2005), complicating the construction of age models."
corrected

Page 9, Lines 31 to 34:
Adding a precession cycle in deep-sea records to the clay layer is not well argued (see specific comments).
It is likely to miss cycles in XRF Ca records because of the clay layer. However, in Fe and Ba XRF data, cycles are well expressed (see ODP Site 690 in Röhl et al., 2007).
This has been addressed already in the major comments above.

Page 10, Lines 5 to 7:
Charles et al. (2011) found 8.5 precession cycles at BH9/05 Core for the entire CIE, similar to Röhl et al. (2007), who used ODP 1263 data.
The recovery recorded in the carbon isotope data of TOC at the BH9/05 Core does not show a rapid but a more gradual recovery. And identification of the inflection "G" is not straight forward and almost impossible. Assuming that the rapid recovery ends at 500m in that section, a relatively small change in the carbon isotope recovery gradient, is 6 precession cycles from the onset. This would imply the same duration for the CIE as the clay layer in the deep sea spanning the onset to rapid recovery. However, we would like not to speculate too much due to the uncertain placement of inflection point "G" and /or in the identification of the rapid recovery extend in the BH9/05 Core.

Page 11, Line 25:
"Fe intensities, core images, and color reflectance data were used ...."
into: "Sedimentary records of Fe intensities, core images, and color reflectance data were used ...."
corrected

Page 19 (Figure 1 caption)
"Location map for ODP sites 702, 1260 and 1263 on a 40 Ma paleogeographic reconstruction in Mollweide projection (from http://www.odsn.de)."
into: "Location map for BBCP (Bighorn Basin Coring Project, Wyoming, USA), ODP Leg 208 (Sites 1260 and 1263) and ODP Leg 113 (Site 690) on a 56 Ma paleogeographic reconstruction in Mollweide projection (from http://www.odsn.de, Hay et al., 1999)."
    should also refer to the original paper of Hay et al. (1999), and not only to the website
corrected and citation added

Page 20 (Figure 2 caption):
The Wilkens et al.'s (submitted) ms referred in Figure 2 caption, but cited in the reference list as Wilkens et al. (2017); the paper already appeared, so should be 2017.
corrected and citation added

Page 23 (Figure 5 caption)
Line 4: '(lines)' into '(solid lines)'
Line 5: 'at the PETM' into 'at the onset of PETM'
corrected

Page 25 (Figure 7 caption)
Line 5: "... extracted Gaussian filter of the PCB XRF Fe intensity data"
would better be "... extracted precession cycles using a Gaussian filter of the PCB XRF Fe intensity data".
    Could the authors please point the end of the CIE directly on δ C data of PCB and deep-sea records?
Corrected and indicated

Synchronizing early Eocene deep-sea and continental records – cyclostratigraphic age models for the Bighorn Basin Coring Project drill cores

Thomas Westerhold[1], Ursula Röhl[1], Roy H. Wilkens[2], Philip D. Gingerich[3], William C. Clyde[4], Scott L. Wing[5], Gabriel J. Bowen[6], Mary J. Kraus[7]

[1]MARUM – University of Bremen, Bremen, 28359, Germany
[2]Hawaii Institute of Geophysics & Planetology, University of Hawaii, Honolulu, HI, 96822, U.S.A.
[3]Museum of Paleontology, University of Michigan, Ann Arbor, Michigan 48109-1079, U.S.A.
[4]Department of Earth Sciences, University of New Hampshire, 56 College Rd., Durham, NH 03824, U.S.A.
[5]Department of Paleobiology, P.O. Box 37012; National Museum of Natural History, Smithsonian Institution, Washington, D.C. 20013 U.S.A.
[6]Department of Geology & Geophysics, University of Utah, Salt Lake City, UT, 84112, U.S.A.
[7]Department of Geological Sciences, University of Colorado at Boulder, UCB 399; Boulder, CO80309, U.S.A.

Correspondence to: Thomas Westerhold (twesterhold@marum.de)

Abstract.

A consistent chronostratigraphic framework is required to understand the effect of major paleoclimate perturbations on both marine and terrestrial ecosystems. Transient global warming events in the early Eocene, 56-54 Ma ago, show the impact of large scale carbon input into the ocean-atmosphere system. Here we provide the first time-scale synchronization of continental and marine deposits spanning the Paleocene-Eocene Thermal Maximum (PETM) and the interval just prior to the Eocene Thermal Maximum 2 (ETM-2). Cyclic variations in geochemical data come from continental drill cores of the Bighorn Basin Coring Project (BBCP, Wyoming, USA) and from marine deep-sea drilling deposits retrieved by the Ocean Drilling Program (ODP). Both are dominated by eccentricity modulated precession cycles used to construct a common cyclostratigraphic framework. Integration of age models results in a revised astrochronology for the PETM in deep-sea records that is now generally consistent with independent [3]He age models. The duration of the PETM is estimated at ~200 kyr for the CIE and ~120 kyr for the associated pelagic clay layer. A common terrestrial and marine age model shows a concurrent major change in marine and terrestrial biotas ~200 kyr before ETM-2. In the Bighorn Basin, the change is referred to as Biohorizon B, and represents a period of significant mammalian turnover and immigration, separating the upper *Haplomylus-Ectocion* Range Zone from the *Bunophorus* Interval Zone and approximating the Wa-4–Wa-5 land mammal zone boundary. In sediments from ODP Site 1262 (Walvis Ridge), major changes in the biota at this time are documented by the radiation of a "2nd generation" of apical spine-bearing sphenoliths species (e.g., *S. radians* and *S. editus*), the emergence of *T. orthostylus*, and the marked decline of *D. multiradiatus*.

1 Introduction

Early Eocene greenhouse climate on Earth was punctuated by transient global warming events (Cramer et al., 2003; Kirtland-Turner et al., 2014). The Paleocene-Eocene Thermal Maximum (PETM or Eocene Thermal Maximum 1: ETM1) at 55.93 Ma (Kennett and Stott 1991; Koch et al., 1992; Bowen et al., 2001; Zachos et al., 2005; Bowen et al., 2015) is the most pronounced hyperthermal event, with a ~5-8°C global warming (McInerney and Wing, 2011). The Elmo event (aka ETM2 or H1) (Cramer et al., 2003; Lourens et al., 2005) is another prominent transient warming event at 54.05 Ma (Westerhold et al. 2017). Both have been studied in great detail in deep-sea and terrestrial sedimentary successions (e.g., Zachos et al., 2005; Abels et al., 2016).

The hyperthermal events in outcrops and ocean drill cores can be identified by the characteristic negative carbon isotope excursions (CIEs), although these differ in magnitude (McInerney and Wing, 2011; Sluijs and Dickens, 2012; Bowen, 2013). The CIEs are interpreted to be due to massive inputs of ^{13}C-depleted carbon to the exogenic carbon pool (see Dickens et al., 2011 for discussion). For both events, major changes in land and ocean biotas have been documented (McInerny and Wing, 2011; Slujis et al., 2007). In the fossil record, the PETM, for example, marks the appearance of the modern order of mammals including horses and primates on land (Gingerich, 1989; Gingerich, 2006) and a major extinction of benthic foraminifera in the deep sea (Thomas, 1989).

The hyperthermals provide important evidence for understanding the dramatic and long-lasting consequences of a rapid massive input of CO_2 into the ocean-atmosphere system within a few thousand years (Kirtland-Turner and Ridgwell, 2016; Zeebe et al., 2016). The PETM in particular, the largest CIE of the last 100 million years, is very important for understanding Earth's future climate (McInerney and Wing, 2011), but the anthropogenic input of CO_2 may be as much as an order of magnitude more rapid than at the PETM (Zeebe et al., 2016).

Key records for studying the early Eocene climate and hyperthermals come from carbonate rich deep-sea drill cores from Walvis Ridge in the South Atlantic (Zachos et al., 2005) and terrestrial fluvial deposits with paleosols in the Bighorn Basin in Wyoming, USA (Koch et al., 1992; Bowen et al., 2001, 2015; Abels et al., 2012; Abels et al., 2016). Deep-sea records have much lower sedimentation rates, in the order of cm/kyr compared to the terrestrial records having sedimentation rates in the order of m/kyr, but have been deposited continuously. Sedimentation in terrestrial environments was very likely more dynamic due to the different types of deposition (see Bowen et al., 2015). To interpret rates of changes of geological processes before, during and after the events a detailed age model is required. Deep-sea records around the PETM and Elmo event reveal extraordinary cyclicity related to precession and eccentricity of the Earth's orbit that was used for establishing high-resolution age models based on cyclostratigraphy and astronomical tuning (Lourens et al., 2005; Röhl et al., 2000, 2007; Westerhold et al., 2007; Abdul Aziz et al., 2008; Stap et al., 2009). Cyclostratigraphic estimates of the duration of the PETM from deep-sea records are hampered by the lack of carbonate-rich sequences, which are characterized on sites nearby

2

Gelöscht: major

Gelöscht: Both have been studied in great detail in both in deep-sea sedimentary and terrestrial successions (Zachos et al., 2005; Abels et al., 2016)

Gelöscht: as

Gelöscht: δ

Gelöscht: The CIEs are interpreted as massive inputs of δ^{13}C-depleted carbon to the exogenic carbon pool (see Dickens et al., 2011 for discussion)

Gelöscht: the future of climate on Earth

Gelöscht: Deep-sea records have a much lower sedimentation rate (cm/kyr) compared to the terrestrial records (m/kyr),

Gelöscht: Sedimentation at the terrestrial successions very likely was more dynamic due to the different types of deposition (see Bowen et al., 2015).

Gelöscht: To interpret rates of changes and processes before, during and after the events a detailed age model is required.

the paleo-CCD with a clay- rich layer at the onset of the event (Röhl et al., 2007), resulting from severe carbonate dissolution (Zachos et al., 2005). Alternative age models based on extraterrestrial [3]He assign more time to the clay layer and a more rapid recovery to pre-PETM δ^{13}C values than do cyclostratigraphic models (Murphy et al., 2010). The stacking pattern of paleosols in the terrestrial PETM section at Polecat

5　Bench is driven by climatic precession and therefore was used to develop an astronomical age model for the CIE (Abdul-Aziz et al., 2008). Cyclicity in outcrops of fluvial deposits prior to and during the Elmo event in the Bighorn Basin was dominated by precession (Abels et al., 2012; Abels et al., 2013), similar to what has been found in deep-sea sediments (Lourens et al., 2005; Westerhold et al., 2007; Zachos et al., 2010; Littler et al., 2014).

10　Because records from both realms show precession-dominated cyclicity it should be possible to correlate and synchronize them. In summer 2011, the Bighorn Basin Coring Project (BBCP) drilled 900 m of overlapping cores from three sites covering the interval of the PETM and Elmo events (Clyde et al., 2013). The BBCP retrieved continuous unweathered material for common multiproxy studies. The main purpose of this report is to establish high-resolution age models for the BBCP drill cores based on

15　cyclostratigraphy and integrate existing age models from outcrops. Second, these new BBCP age models will be combined with deep-sea records to synchronize and improve the available astronomical age model for the PETM and Elmo interval. The new age models will allow other studies to compare multiple proxy records from both realms at unprecedented temporal accuracy. Our study also allows us to consider whether the mammalian turnover called "Biohorizon B" in the Bighorn Basin fossil faunas (Schlanker,

20　1980; Chew and Oheim, 2009; Chew and Oheim, 2013; Chew, 2015) is synchronous with changes in deep-sea calcareous nannofossil assemblages (Agnini et al., 2007) significantly prior to the Elmo event.

2 Material and Methods

The BBCP drilled late Paleocene to early Eocene fluvial deposits including the PETM at Polecat Bench (PCB) and Basin Substation (BSN), and the Elmo interval at Gilmore Hill (GMH) (Fig.1, Clyde et al.,

25　2013). Two overlapping holes were drilled at BSN down to 138.4 mbs (BSN11-1A) and 138.6 mbs (BSN11-1B). At PCB two overlapping holes were drilled to 130 mbs (PCB11-2A) and 245.1 mbs (PCB11-2B). At GMH one hole was drilled down to 202.4 mbs (GMH11-3A) and a second down to 66.7 mbs (GMH11-3B). All cores were split and processed according to IODP standards that included visual core description, color and line-scanning, sampling for post party investigations at home laboratories, and

30　archiving at the Bremen Core Repository during a BBCP Science Party at MARUM, University Bremen, Germany, in January 2012 (Clyde et al., 2013).

Here we present the results of processing and interpreting line scan images and color reflectance data for the BSN, GMH and PCB sites, with the records from PCB being presented initially in Bowen et al. (2015). All cores from PCB, BSN and GMH were XRF scanned over the course of 2012 at MARUM, University

3

of Bremen, and we use the iron (Fe) intensity data here as well. XRF data were collected every 2 cm down-core using XRF core scanner 3 (AVAATECH Serial No. 12) at MARUM – University Bremen, over a 1.2 cm^2 area with a down-core split size of 10 mm using a generator settings of 50, 30 and 10 kV, a respective current of 1.0, 1.0 and 0.2 mA, and a sampling time of 10 seconds in each run directly at the

5 split core surface of the archive half. The split core surface was covered with a 4-micron thin SPEXCerti Perp Ultralene1 foil to avoid contamination of the XRF detector-prism and desiccation of the cores. The data were acquired by a Canberra X-PIPS Silicon Drift Detector (SDD; Model SXD 15C-150-500) with 150eV X-ray resolution, the Canberra Digital Spectrum Analyzer DAS 1000 and an Oxford Instruments 100W Neptune X-ray tube with a Rhodium (Rh) target. Raw data spectra were processed by the Analysis

10 of X-ray spectra by Iterative Least square software (WIN AXIL) package from Canberra Eurisys. Core data and images have been correlated and integrated using the new software tool CODD (Code for Ocean Drilling Data, Wilkens et al. 2017). This tool greatly facilitates handling of large and complex data sets and allows use of core images for scientific analysis.

Pedogenic carbonate nodules for isotope analysis were identified as discrete, small (~2mm to >5cm in

15 diameter), well-cemented, rounded to sub-rounded accumulations of micritic carbonate, some of which contain observable secondary, diagenetic spar. Samples larger than ~1 cm diameter were slabbed to expose a clean flat surface. For smaller samples, the exterior surface of the nodule was etched using a dental drill. Primary micrite was collected with a dental drill under a binocular microscope. Carbon isotope data acquisition is the same as presented in the supplement of Bowen et al. (2015). Repeatability

20 of the pedogenic carbonate analyses averaged 0.20‰ for δ^{13}C and 0.24‰ for δ^{18}O based on replicate analyses of pedogenic carbonate samples. Isotopic data for PCB nodules were previously reported in Bowen et al. (2015).

All data and tables from this study are open access available at Pangaea Database https://doi.pangaea.de/10.1594/PANGAEA.875685.

25 **3 Results**

3.1 Color reflectance data, XRF core scanning data and composite depth

Weathering resulted in brighter, yellowish colors within the upper ~30 meters of the BBCP drill cores (Fig. 2 in Clyde et al., 2013). Below the weathering zone, sediments appear light to dark gray with reddish to purplish colored paleosols. Lightness varies between 20-60% for all sites with a high degree of

30 variability. a* (red/green) values for PCB and BSN cores range from 0 with values up to 10 or higher in reddish and purplish paleosols. a* values of the GMH cores show higher variability due to the more reddish, varying lithology. b* (blue/yellow) values vary more in the upper 30 meters of the cores in line with the more yellow colors of the weathered zone. Fe core scanning intensities vary between several 1000 up to 100000 total counts (area) and display cyclic changes with a much better signal to noise ratio

4

than the color data. BSN Fe intensities reveal lower variability than PCB and GMH, but higher Fe peaks are more common. GMH and PCB Fe data show persistent cyclicity throughout the succession.

Core images, color reflectance and Fe data have been utilized to correlate between parallel holes for PCB, BSN, and GMH drill cores. As normal shipboard routine for multiple holes drilled by IODP, cores of the

5 BBCP were offset from the original drilling depth (mbs) and subsequently combined. The correlation of the two PCB records and the resulting composite can be found in Bowen et al., (2015, their Fig. 1). Lithological logs, core images, color reflectance CIE L*a*b* from the BBCP Science Party (Clyde et al., 2013), and XRF core scanning Fe intensity for BSN, GMH, and PCB are provided in supplementary Figures S1, S2 and S3 and data tables S1-S6.

10 **3.2 Time-series analysis of BBCP drill cores**

Evolutionary Power Spectra were calculated for the XRF score scanning Fe intensities and color reflectance a* (AStar) data for all drill holes separately. Before spectral analysis, the raw data were re-sampled and the trend removed. On the residual data Multitaper Method (MTM) spectra were calculated using the mtmML96 routine of the 'Astrochron' software package (Meyers 2014). Cycles identified by

15 MTM spectrum analysis were then extracted by a Gaussian bandpass filter of the central frequency with 30% bandwidth using AnalySeries (Paillard et al., 1996).

3.2.1 Polecat Bench

At PCB, the dominant cycles in Fe intensity data are 8.2, 3.45, 1.2, 1.02 and 0.58 m long (Fig. 2), and in the a* data 7.8-8, 3.45 and 1.1m (Fig. S6). This result is consistent with the observation of 7.7, 3.3 and

20 1.1 m long cycles in a* data obtained from the outcrop (Abdul-Aziz et al., 2008). The slight difference in length could be due to thickness variations of paleosols and sandstone beds between the drill site location and the outcrop. The two longer cycles around 8 and 3.5m have been interpreted as precession and sub-precession or millennial-scale cycles (see Abdul-Aziz et al., 2008). Assuming that the 8.2 m cycles represent the averaged 21 kyr long precession cycle, the other cycles have a period of 8.83, 3.1, 2.61 and

25 1.48 kyrs, respectively. The evolutionary spectra show some slight changes in the length of the dominant cycles around 8 m which can be interpreted as changes in sedimentation rate.

3.2.2 Basin Substation

At BSN, a range of dominant cycles in Fe intensity are apparent (6.8, 3.3, 2, 1.7, 1.25, 1.05 and 0.58 m, Fig. 3). In the a* data, a similar variety can be observed (Fig. S7). The evolutionary spectra show that

30 cycles are not persistent over the entire succession, hampering the construction of a cyclostratigraphic age model at BSN. These irregularities in cyclicity could point to strong changes in sedimentation rate, condensed intervals in the record, and/or changes in the processes regulating the Fe content in the sediment. Relatively stable cycles can be observed in the interval from 50 to 85 m, with dominant 6.8 m

cycles that might correspond to the precession cycles with ~8 m length in the PCB core. Because the cycles are not persistent for the entire drill core, a cyclostratigraphy for BSN was not established here.

3.2.3 Gilmore Hill

At GMH the dominant cycles in Fe intensity and a* data are 7.5-6.7, 3.3, 2.5, ~1m and 0.62 m long (Fig. 2, Fig. S7). The evolutionary spectra show relatively regular cycles just before the Elmo event (see discussion below), which is cut out by sandstones of a channel fill at 0-20 m. Below this, the dominant cycle undulates around 7 m and is clearly visible in the data. Long-term sediment accumulation rates in the closest outcrop section with magnetostratigraphy (Clyde et al., 1994; Clyde et al., 2007) suggest that 7 meters of sediment in this part of the basin represents between 14,500 and 25,500 years and thus is consistent with precession. The 7 m and 3.3 m long cycles are also consistent with precession and half-precession cycles observed in a* values from the Bighorn Basin Deer Creek Amphitheater section, which is ~17km away along the McCullough Peaks escarpment (Abels et al., 2013). Thus these cycles can be used for building a cyclostratigraphy.

4 Cyclostratigraphy - Linking outcrops and BBCP drillcores

The obtained data allow the construction of a cyclostratigraphy for drill cores from GMH and PCB. We correlated GMH and PCB records with outcrop successions to allow full integration of Bighorn Basin surface-derived data with the drill cores.

4.1 Age model for PCB PETM

For the PCB drill cores, a correlation to a composite outcrop (Abdul Aziz et al., 2008) is already available (Bowen et al., 2015) identifying well-known local marker beds consisting of red to purplish paleosols. The rhythmic stacking pattern of the paleosols is driven by orbital precession cycles and was successfully used to establish a cyclostratigraphy for the PETM at Polecat Bench (Abdul Aziz et al., 2008) roughly consistent with independent age models from deep sea cores (Farley and Eltgroth, 2003; Röhl et al., 2007). For the PCB cores a set of pedogenic age models was developed calculating time based on thickness, sediment type, and paleosol maturity of individual stratigraphic units (Bowen et al., 2015), but no cyclostratigraphy similar to the outcrop has been developed so far.

The cyclostratigraphy for PCB cores presented here is based on cycle counting of both the a* and XRF Fe data cycles that are interpreted to be related to precession. Precession and sub-precession or millennial-scale cyclicity was extracted by Gaussian filtering of a* and XRF Fe data (Figure 5) with the Fe data providing a much cleaner rhythmic signal due to the better signal to noise ratio compared to a*. Taking the soil nodule carbon isotope data (Bowen et al., 2015) as reference, we started counting at the onset of the PETM CIE (see Figure 5), with positive numbers up-core and negative numbers down-core. The filter of the precession cycles of ~8.2 m in both data sets show modulations that are consistent with eccentricity.

We estimate that the PCB core covers 33 precession cycles, of which we use 29 for a direct age assignment. Cycles -10, -11, -13 and -14 are hard to identify because of the low amplitude variation in the data. This observation is consistent with lower amplitudes in a* and XRF Fe data 300 kyr prior to the onset of the PETM in deep-sea sediments from Walvis Ridge (South Atlantic) and Blake Nose (North

5 Atlantic) (Westerhold et al., 2007) caused by a minimum in the long 405-kyr eccentricity cycle.

For each of the precession cycles we assume a constant duration of 21 kyr as done in previous deep-sea cyclostratigraphic models (Röhl et al., 2007; Westerhold et al., 2007) setting the onset of the PETM as 0. Relative ages with respect to the onset of the PETM are given in table 1. For absolute ages we use the age for onset of the PETM as 55.930 Ma (Westerhold et al., 2007; Westerhold et al., 2015) and add or subtract

10 the relative age. According to the filter of the a* and Fe data, we also arbitrarily assume that the onset of the PETM is located in the minimum between cycle -1 and 1 (Figure 5). Regarding the phase relationship, whether paleosols correspond to precession minima or maxima (Abels et al., 2013) is unknown and not relevant for establishing a cyclostratigraphy based on cycle counting itself. For simplicity we assume that paleosols correspond to more negative bulk carbonate carbon isotope values in more clay rich layers in

15 the deep-sea records (higher Fe XRF intensities, Zachos et al., 2010; Littler et al., 2014; Zeebe et al. 2017). Thus, the onset of the PETM was set into a precession minimum in the PCB cyclostratigraphy model. The new cyclostratigraphy is almost identical to the outcrop model (Abdul-Aziz et al., 2008) for the PETM. Because we use the longer drill core from PCB now as a reference, minor discrepancies between outcrop and drill core paleosol and sandstone bed thicknesses had to be corrected in the tie points

20 for the outcrop (Abdul-Aziz et al., 2008). This did not affect the original estimates for the duration of the PETM CIE and rapid recovery reported in Abdul-Aziz et al. (2008). The new cyclostratigraphic age model for PCB covers a longer stretch across the PETM compared to previous outcrop studies spanning from the latest Paleocene precession-cycle -15 (as in Westerhold et al., 2007) to early Eocene precession-cycle 15: 56.234 to 55.626 Ma with the PETM at 55.930 Ma.

25 **4.2 Age model for GMH – pre Elmo interval**

Extensive outcrop work and cyclostratigraphic interpretations are also available for terrestrial sediments across the ETM-2 (Elmo, Lourens et al., 2005) in the Bighorn Basin (Clyde et al., 1994; Clyde et al., 2007; Abels et al., 2012; Abels et al., 2013; Abels et al., 2016; D'Ambrosia et al., 2017). Alluvial sedimentary cycles before and after the Elmo are shown to be precession forced (Abels et al., 2012). The

30 GMH cores cover an interval prior to the ETM-2, which is cut out by a sandstone channel complex (Clyde et al., 2013). To establish a cyclostratigraphy for the GMH drill cores, precession and half-precession cycles were extracted from the a* and XRF Fe data (Figure 6). Both data sets show high amplitude variations as expected from the more reddish terrestrial deposits. The extracted a* and XRF Fe data cycles are consistent with previous cyclic variations in a* values from outcrop samples. The drill core data have

35 been correlated to the Deer Creek (Fig. S9, Abels et al., 2012) and Gilmore Hill (Fig. S10, D'Ambrosia

7

et al., 2017) sections using prominent purple marker beds and field observations. Subsequently, we adopted the labelling system of Abels et al. (2013, A-P) but extend it towards the ETM-2 at GMH (Q to Y). As already observed in the PCB drill cores, data from the GMH core show the same precession length and amplitude modulation as observed in outcrop samples (Fig. S9). Combining the correlation to the

5 outcrop interpretation with the precession-filtered data from the drill cores we established a best fit cycle counting age model for GMH drill cores. This is necessary because the filter of a* and Fe data are not consistent in all parts of the record. Basic tie-points for correlation and cyclostratigraphy are given in table 2. For a relative age model we assigned the precession cycle numbers identified in Walvis Ridge ODP sites from Leg 208 and their relative age to the onset of the PETM (Westerhold et al., 2007) to the

10 precession cycles found in GMH. For absolute ages we provide one option which refers to the age of 55.930 Ma for the onset of the PETM (see PCB) and another option relative to the age of 54.05 Ma for ETM-2. The age model suggests that the GMH cores cover precession cycles -A to Y, representing roughly 500 kyrs of terrestrial deposition from 54.596 to 54.071 Ma.

5 Discussion

15 This study not only provides a high resolution cyclostratigraphic age model for the BBCP drill cores but also improves existing age models for the interval spanning the PETM and prior to ETM-2. BBCP drill core and Bighorn Basin outcrops are an ideal basis for revision of the PETM age model that is mainly derived from deep-sea sediments with low sedimentation rates. Dissolution of carbonate, particularly at the onset of the PETM, hampers the establishment of a complete chronology for the PETM from marine

20 cores (Kelly et al., 2005; Kelly et al., 2010). Uncertainty in correlation between terrestrial successions from the Bighorn Basin and marine records also makes it difficult to evaluate if the terrestrial Biohorizon B is synchronous with major changes in marine calcareous nannofossil assemblages prior to ETM-2 (Agnini et al., 2007). Bighorn Basin deposits of the Fort Union and Willwood formations with their extremely high sedimentation rates allow very detailed insight to changes in biota on land. Using our new

25 astrochronology we can test if these biotic turnovers were coeval in marine and terrestrial ecosystems.

5.1 Synchronizing deep-sea and continental records for the PETM

Precession related variations in XRF core scanning data (Röhl et al., 2000; Röhl et al., 2007) on the one hand, and the concentration of extraterrestrial ^{3}He in ODP cores from the same regions (Farley and Eltgroth 2003; Murphy et al., 2010) were used to develop an age model for the PETM from pelagic

30 sequences. During the PETM, massive dissolution of carbonates in the deep sea truncated the cyclostratigraphic record (Zachos et al., 2005), complicating the construction of age models. Cyclostratigraphy and extraterrestrial ^{3}He age models are roughly consistent but show some discrepancies in the duration and recovery of the CIE (Murphy et al., 2010). The extraterrestrial ^{3}He age model proposed $217^{+44/-33}$ kyr for the entire CIE compared to 171 kyr by cyclostratigraphy (Röhl et al., 2007; Murphy et

8

al., 2010). The duration of the clay layer, which is the interval between the sharp contact of dissolution at the onset and the recovery of carbonate content to pre-event levels (Figure 7), was estimated to be $167^{+43/-24}$ kyr by extraterrestrial ^{3}He (Murphy et al., 2010) and ~95 kyr by cyclostratigraphy (Röhl et al., 2007). The helium age model can be compromised if the flux of extraterrestrial ^{3}He was not constant during the

5   PETM. Orbital chronology depends on the correct recognition of all sedimentary cycles, which is notoriously difficult at the onset of the PETM. Severe carbonate dissolution, including the burn-down of carbonate deposited before the actual ocean acidification during the onset of the PETM (Zeebe and Zachos, 2007), could explain the difference in these estimates of the PETM duration. In addition, cyclostratigraphic work around the deep-sea PETM sections (Röhl et al., 2007; Westerhold et al., 2007)

10   limits the maximum duration of the clay layer to 7 precession cycles, or 147 kyr, which is within the error of the ^{3}He age model (210-143 kyr, Murphy et al., 2010).

At the Walvis Ridge ODP sites, the top of the clay layer coincides with the top of the initial rapid recovery of the CIE (Recovery phase I in Murphy et al., 2010). To correlate deep-sea and terrestrial records, the onset and the top of the initial rapid recovery of the CIE are commonly used (McInerney and Wing, 2011).

15   The PCB cyclostratigraphy indicates that the duration of this interval mentioned above covers six precession cycles or ~120 kyr (assuming an average duration of 21 kyr for one precession cycle). This duration is between the estimates of 90 and 135 kyr used as a basis for the age model in Bowen et al. (2015). As a consequence, a duration of 120 kyr suggests that the deep-sea records (~95 kyr) are missing ~25 kyr or about one precession cycle at the onset of the event. The onset of the PETM was set into a

20   precession minimum in the PCB cyclostratigraphy model (see above), and thus subtracting 21kyr (one precession cycle) from the missing ~25 kyr leaves us with additional ~4 kyr on top of the missing precession cycle in the duration compared to the deep sea. If we compare the PCB CIE of our new cyclostratigraphy to the deep-sea CIE using the existing orbital chronology (Röhl et al., 2007) and aligning the records at the onset of the PETM, the initial recovery from sustained minimum δ^{13}C values

25   will be offset by ~25 kyr. A lag of 25kyr between this major inflection in the ocean and atmosphere carbon isotope records is not possible given the rapid rate of carbon exchange between the atmosphere and surface (10's of years) and deep (100's of years) ocean reservoirs (Revelle and Suess, 1957; Broecker and Peng, 1982; Bowen, 2013). We therefore modified and updated the age model of Röhl et al., (2007) from precession cycles -20 to 20 (56.320 to 55.520 Ma) by adding a precession cycle at the onset of the

30   PETM and moving the onset of the PETM between two precession cycles (see Table 1, Fig. 7 and S12). As a result of the updated orbital chronology, the duration of the clay layer now is estimated to be ~120 kyr, and the total duration of the PETM is ~200 kyr, compared to the previous 95 and 171 kyr estimates (Röhl et al., 2007). Comparing the duration of the entire CIE of the PETM and understanding subtle differences between age models requires some discussion about the definition of PETM phases. The onset

35   of the PETM CIE is relatively easy to identify in many different records. The termination of the CIE at Site 1263 and the Site 690 reference section were defined (Tables 1 and 2) by identifying an inflection

9

point in the bulk carbon isotope curve (Röhl et al. 2007). The inflection point was labeled "G" in Zachos et al. 2005 and used for correlation to other records. It is located at 167.12 mbsf in ODP 690 (Zachos et al. 2005). Using the Röhl et al. (2007) age model this point is 153.5 kyr after the onset of the PETM (Table 2 of Röhl et al., 2007; not 171 kyr as written in Murphy et al. 2010). Using the updated age model

5 developed in this study we obtain an age of 55.749 Ma for inflection point G which translates into 182 kyr between onset and end CIE (Figure 7). But the end of the recovery as outlined in Röhl et al. (2007) is between cycle 8 and 9 at ODP 690. Based on cycle counting, the duration of the CIE is roughly 170 kyr (8*21=168) as determined in that paper. In our revision of the age model we simply added one precession cycle, therefore the duration of the PETM sensu Röhl et al. (2007) is roughly 190 kyr (9*21=189 kyr). In

10 addition, the position of the onset of the PETM in our manuscript was placed between two precession cycles adding another 7 kyr to the duration (relative age of precession cycle 2 in Röhl et al. 2007 is 24 kyr after the onset of the PETM, in our study it is 31 kyr after onset). Summing up, the PETM CIE duration is roughly 200 kyr (189+7=196 kyr) using the commonly used definition for deep-sea records (Zachos et al., 2005; Röhl et al. 2007). Identification of inflection point G defined in the deep-sea

15 reference record of Site 690 in the PCB core and/or outcrop is not possible preventing any comparable estimate for the entire CIE of the PETM as defined in the deep-sea. Nevertheless, records from both realms have the same duration of ~120 kyr from onset CIE to the end of the rapid recovery, equivalent to the clay layer in the deep-sea or the interval from key event I to IV in Zachos et al. (2005).

The updated duration of the CIE in the deep-sea using cyclostratigraphy is in agreement now with the

20 [3]He age model (Farley and Eltgroth, 2003; Murphy et al., 2010), but the duration of the clay layer is still more than 23 kyr shorter. Although the overall cyclostratigraphy around the PETM (Röhl et al., 2007; Westerhold et al., 2007) would allow a seventh precession cycle in the clay layer, there is no indication in the Bighorn Basin records for a missing precession cycle at the onset of the event. Six cycles in the PETM CIE have also been reported from the BH9/05 drill core of the Paleocene-Eocene boundary in

25 Spitsbergen (Charles et al., 2011; cyclostratigraphic option B therein). U/Pb dating for the onset of the PETM from the Spitsbergen record (55.866 ± 0.098 Ma) is also consistent with the 55.930 ± 0.05 Ma estimate from astronomical calibration (Westerhold et al., 2008; Westerhold et al., 2015).

Direct comparison of the [3]He age model (Murphy et al., 2010) and our orbital chronology for Site 1266 (Fig. S13) shows that the initial rapid recovery located in precession cycle 6 of the PCB record is, on

30 average, offset by 40 kyr in the [3]He age model. For calibration of the constant extraterrestrial [3]He flux, a average sedimentation rate between 306.92 and 308.54 mcd at Site 1266 of 1.43 cm/kyr based on the age model of Röhl et al. (2007) was used. It is important to note that the age model uses the average duration for precession of 21 kyr. Over hundreds of millions of years, the Moon moved away from Earth and the rotation of the Earth slowed down with time, changing the precession frequency of Earth (Laskar et al.,

35 2004). As a consequence, the average precession cycle at 56 Ma will not be 21kyr but rather 20.5 kyr. This subtle difference could point to the fact that, in the calibration interval of the 6 precession cycles

10

Gelöscht: the	
Gelöscht: r	
Gelöscht: on average	

used for the extraterrestrial ³He flux estimate, there is less time and therefore the sedimentation rates are a bit higher, on the order of 1.5 cm/kyr. Assuming the decrease in the precession period over time to be valid, the extraterrestrial ³He flux would be higher, resulting in a duration of ~200 kyr for the CIE (306.15 to 304.70 mcd at 1266) and ~160 kyr for the clay layer. The discrepancy would be still hard to explain

5   because to match the duration of the clay layer to the ~120 kyr estimate, the sedimentation rate in the calibration interval has to be increased to 2 cm /kyr resulting in a cycle duration of 14-16 kyr for the six precession cycles. The duration of the CIE would also be reduced to 150-160 kyr, making this scenario rather unlikely. These uncertainties call for more ³He-based studies across the PETM to investigate if there is also time missing in the PCB sections. A relevant additional issue is whether the Helium isotope

10 ratio is affected by the enhanced coeval flood basalt volcanism in East Greenland (Wotzlaw et al., 2012). Until then we consider the updated age model presented here as a proper solution to compare deep sea with terrestrial records.

5.2 Synchronizing deep-sea and continental records prior to the ETM-2

15 Eccentricity modulated precession cycles dominate geochemical records in the interval prior to ETM-2 and have been used to establish cyclostratigraphic age models (Westerhold et al., 2007; Zachos et al., 2010; Littler et al., 2014). To synchronize marine and terrestrial records (GMH), we simply adopted the cyclostratigraphic ages from the deep-sea sections (Fig. 8, Tab. 2). Remarkably, the same eccentricity related amplitude modulation of XRF Fe data can be observed for both records. Low amplitude precession

20 cycles are present from 54.65 to 54.48 Ma followed by high amplitude cyclicity around 54.44 Ma, implying a climate system feedback to modulations in precession affecting both realms (Fig. 6). Variations in the XRF Fe data of the deep sea are most likely driven by changes in carbonate deposition. In the terrestrial sediments these variations have been attributed to large-scale reorganization of the fluvial system driven by astronomically forced changes in the hydrological cycle (Abels et al., 2012). Comparing

25 the stable carbon isotope curves from deep-sea benthic foraminifera, bulk carbonate sediment and soil nodules (Tab. S9) shows similar congruent variations, even outside the extraordinary hyperthermal events (e.g. ETM-2, Abels et al., 2016). Consistent small scale variability clearly is linked to changes in the global carbon cycle.

Knowing that the age model for the deep-sea and the Bighon Basin records are synchronous, we can test

30 for a temporal relation between Biohorizon B in the Bighorn Basin (Clyde et al., 2007) and biotic changes in calcareous nannofossils in deep-sea records. The best constraint on the stratigraphic position of Biohorizon B comes from the Gilmore Hill section where it falls between locality MP167 (LAD of *Haplomylus*) and MP166 (FAD of *Bunophorus*), both of which fall directly in the line of section. The mid-level of locality MP167 is at 807 meters (above PETM) of that section and the mid-level of locality

35 MP166 is 840 meters so Biohorizon B must fall somewhere in the interval between ~807 and ~840 meters

11

of the Gilmore Hill section (see Abels et al., 2012 and D'Ambrosia et al., 2017 for details). Another locality, MP122, that is not located directly in the line of section but has been physically correlated to the 825-835 meter level in this section via bed tracing, contains both *Haplomylus* and *Bunophorus*, so provides a more precise biostratigraphic estimate of Biohorizon B but with additional stratigraphic uncertainty due to the long distance correlation. The 33 meters of section between 807 and 840 meters represent 4-5 precession cycles (#79 to #83 in table 2) from 54.151 to 54.254 Ma and the 10 meters of section between 825 to 835 meters represent 1.5 precession cycles (between #81 and #83, centered at #82 in table 2) from 54.165 to 54.195 Ma.

In sediments from ODP Site 1262 (Walvis Ridge), a series of biotic events, representing rapid evolutionary change, are documented in the calcareous nannofossil assemblage by the radiation of a "2nd generation" of apical spine-bearing sphenoliths species (e.g., *S. radians* and *S. editus*), the emergence of *T. orthostylus*, and the marked decline of *D. multiradiatus* 200 kyr prior to the ETM-2 (Agnini et al., 2007; Figure 8). Based on our GMH cyclostratigraphy, the terrestrial faunal turnover at Biohorizon B occurred coeval with the upper half of the deep-sea biotic events, possibly pointing to a common response of the biota in both realms to environmental change 54.2 Ma ago. However, in high-resolution isotope records from the deep sea (Littler et al., 2014), there is no evidence for a major perturbation or even change in environmental conditions that could cause the synchronous response in the marine and terrestrial ecosystems, but the coincident timing could point to some common response to a forcing yet to be discovered.

6 Conclusions

Sedimentary records of Fe intensities, core images, and color reflectance data were used to build composite records for the Bighorn Basin Coring Project drill cores from Gilmore Hill, Basin Substation, and Polecat Bench. Eccentricity modulated precession scale cyclicity observed in the high-resolution data allowed the construction of cyclostratigraphic age models for GMH and PCB spanning a 500 kyr interval prior to the ETM-2 and a 500 kyr interval across the PETM. The established orbital chronology of the drill core data not only is consistent with previous age models from outcrops, but also helped to improve the cyclostratigraphic age model for the PETM in deep-sea records. Synchronisation and integration of all records define a duration of ~200 kyr for the CIE and ~120 kyr for the clay layer of the PETM, largely consistent with independent ³He age models. XRF and lightness data from marine and terrestrial records show coherent amplitude modulations in both investigated intervals. The combination of marine and terrestrial records on a common age model prior to the ETM-2 point towards a coeval turnover in marine and terrestrial biota likely related to a common but as yet unknown environmental change. The successful synchronizing of marine and terrestrial records using cyclostratigraphy yields potential for future research deciphering climate changes on Earth and the impact on biota at an unprecedented temporal resolution.

12

Acknowledgements

> Formatiert: Nicht Hervorheben
> Formatiert: Nicht Hervorheben
> Formatiert: Nicht Hervorheben
> Gelöscht: (www.pangaea.de) database

References

Abels, H. A., Clyde, W. C., Gingerich, P. D., Hilgen, F. J., Fricke, H. C., Bowen, G. J., and Lourens, L. J.: Terrestrial carbon isotope excursions and biotic change during Palaeogene hyperthermals, Nature Geosci, 5, 10.1038/ngeo1427, 2012.

Abels, H. A., Kraus, M. J., and Gingerich, P. D.: Precession-scale cyclicity in the fluvial lower Eocene Willwood Formation of the Bighorn Basin, Wyoming (USA), Sedimentology, 60, 1467-1483, 10.1111/sed.12039, 2013.

Abels, H. A., Lauretano, V., van Yperen, A. E., Hopman, T., Zachos, J. C., Lourens, L. J., Gingerich, P. D., and Bowen, G. J.: Environmental impact and magnitude of paleosol carbonate carbon isotope excursions marking five early Eocene hyperthermals in the Bighorn Basin, Wyoming, Clim. Past, 12, 1151-1163, 10.5194/cp-12-1151-2016, 2016.

Agnini, C., Fornaciari, E., Raffi, I., Rio, D., Röhl, U., and Westerhold, T.: High-resolution nannofossil biochronology of middle Paleocene to early Eocene at ODP Site 1262: Implications for calcareous nannoplankton evolution, Marine Micropaleontology, 64, 215-248, 10.1016/j.marmicro.2007.05.003, 2007.

Abdul Aziz, H., Hilgen, F. J., van Luijk, G. M., Sluijs, A., Kraus, M. J., Pares, J. M., and Gingerich, P. D.: Astronomical climate control on paleosol stacking patterns in the upper Paleocene–lower Eocene Willwood Formation, Bighorn Basin, Wyoming, Geology, 36, 531-534, 10.1130/g24734a.1, 2008.

Bains, S., Corfield, R. M., and Norris, R. D.: Mechanisms of Climate Warming at the End of the Paleocene, Science, 285, 724-727, 10.1126/science.285.5428.724, 1999.

Bowen, G. J., Koch, P. L., Gingerich, P. D., Norris, R. D., Bains, S., and Corfield, R. M.: Refined Isotope Stratigraphy across the Continental Paleocene-Eocene Boundary on Polecat Bench in the Northern Bighorn Basin, in: Paleocene-Eocene Stratigraphy and Biotic Change in the Bighorn and Clarks Fork Basins, Wyoming, edited by: Gingerich, P. D., University of Michigan Papers on Paleontology, 73-88, 2001.

> Gelöscht: DOI

13

Bowen, G. J.: Up in smoke: A role for organic carbon feedbacks in Paleogene hyperthermals, Global and Planetary Change, 109, 18-29, http://dx.doi.org/10.1016/j.gloplacha.2013.07.001, 2013.

Bowen, G. J., Maibauer, B. J., Kraus, M. J., Röhl, U., Westerhold, T., Steimke, A., Gingerich, P. D., Wing, S. L., and Clyde, W. C.: Two massive, rapid releases of carbon during the onset of the Palaeocene-Eocene thermal maximum, Nature Geosci, 8, 44-47, 10.1038/ngeo2316, 2015.

Broecker, W.S., Peng, T.-H.: Tracers in the sea. Lamont-Doherty Geological Observatory, 690 pp., 1982.

Charles, A. J., Condon, D. J., Harding, I. C., Pälike, H., Marshall, J. E. A., Cui, Y., Kump, L., and Croudace, I. W.: Constraints on the numerical age of the Paleocene-Eocene boundary, Geochem. Geophys. Geosyst., 12, Q0AA17, 10.1029/2010gc003426, 2011.

Chew, A.E.: Paleoecology of the early Eocene Willwood mammal fauna from the central Bighorn Basin, Wyoming. Paleobiology 35, 13–31, 2009.

Chew, A. E., and Oheim, K. B.: Diversity and climate change in the middle-late Wasatchian (early Eocene) Willwood Formation, central Bighorn Basin, Wyoming, Palaeogeography, Palaeoclimatology, Palaeoecology, 369, 67-78, http://dx.doi.org/10.1016/j.palaeo.2012.10.004, 2013.

Chew, A. E.: Mammal faunal change in the zone of the Paleogene hyperthermals ETM2 and H2, Clim. Past, 11, 1223-1237, 10.5194/cp-11-1223-2015, 2015.

Clyde, W. C., Stamatakos, J., and Gingerich, P. D. : Chronology of the Wasatchian land-mammal age: magnetostratigraphic results from the McCullough Peaks section, northern Bighorn Basin, Wyoming. Journal of Geology 102:367-377, 1994.

Clyde, W. C., Hamzi, W., Finarelli, J. A., Wing, S. L., Schankler, D., and Chew, A.: Basin-wide magnetostratigraphic framework for the Bighorn Basin, Wyoming, GSA Bulletin, 119, 848-859, 2007.

Clyde, W. C., Gingerich, P. D., Wing, S. L., Röhl, U., Westerhold, T., Bowen, G., Johnson, K., Baczynski, A. A., Diefendorf, A., McInerney, F., Schnurrenberger, D., Noren, A., Brady, K., and the, B. S. T.: Bighorn Basin Coring Project (BBCP): a continental perspective on early Paleogene hyperthermals, Sci. Dril., 16, 21-31, 10.5194/sd-16-21-2013, 2013.

Cramer, B. S., Wright, J. D., Kent, D. V., and Aubry, M.-P.: Orbital climate forcing of d13C excursions in the late Paleocene - Eocene (chrons C24n-C25n), Paleoceanography, 18, 1097, 10.1029/2003PA000909, 2003.

Dickens, G. R.: Down the Rabbit Hole: toward appropriate discussion of methane release from gas hydrate systems during the Paleocene-Eocene thermal maximum and other past hyperthermal events, Clim. Past, 7, 831-846, 10.5194/cp-7-831-2011, 2011.

D'Ambrosia, A. R., Clyde, W. C., Fricke, H. C., Gingerich, P. D., and Abels, H. A.: Repetitive mammalian dwarfing during ancient greenhouse warming events, Science Advances, 3, 10.1126/sciadv.1601430, 2017.

Farley, K. A., and Eltgroth, S. F.: An alternative age model for the Paleocene-Eocene thermal maximum using extraterrestrial 3He, Earth and Planetary Science Letters, 208, 135-148, 2003.

14

Gingerich, P. D.: New earliest Wasatchian mammalian fauna from the Eocene of northwestern Wyoming: composition and diversity in a rarely sampled high-floodplain assemblage. University of Michigan Papers on Paleontology, 28, 1-97. http://hdl.handle.net/2027.42/48628, 1989.

Gingerich, P. D.: Environment and evolution through the Paleocene-Eocene thermal maximum, Trends in Ecology & Evolution, 21, 246-253, 2006.

Hay, W. W., DeConto, R., Wold, C. N., Wilson, K. M., Voigt, S., Schulz, M., Wold-Rossby, A., Dullo, W.-C., Ronov, A. B., Balukhovsky, A. N., and Soeding, E.: Alternative Global Cretaceous Paleogeography, in: The Evolution of Cretaceous Ocean/Climate Systems, edited by: Barrera, E., and Johnson, C., Geological Society of America Special Paper, 1-47, 1999.

Kelly, D. C., Zachos, J. C., Bralower, T. J., and Schellenberg, S. A.: Enhanced terrestrial weathering/runoff and surface ocean carbonate production during the recovery stages of the Paleocene-Eocene thermal maximum, Paleoceanography, 20, 10.1029/2005PA001163, 2005.

Kelly, D. C., Nielsen, T. M. J., McCarren, H. K., Zachos, J. C., and Röhl, U.: Spatiotemporal patterns of carbonate sedimentation in the South Atlantic: Implications for carbon cycling during the Paleocene-Eocene thermal maximum, Palaeogeography, Palaeoclimatology, Palaeoecology, 293, 30-40, 10.1016/j.palaeo.2010.04.027, 2010.

Kennett, J. P., and Stott, L. D.: Abrupt deep sea warming, paleoceanographic changes and benthic extinctions at the end of the Paleocene, Nature, 353, 225-229, 1991.

Kirtland Turner, S., Sexton, P. F., Charles, C. D., and Norris, R. D.: Persistence of carbon release events through the peak of early Eocene global warmth, Nature Geosci, 7, 10.1038/ngeo2240, 2014.

Kirtland Turner, S., and Ridgwell, A.: Development of a novel empirical framework for interpreting geological carbon isotope excursions, with implications for the rate of carbon injection across the PETM, Earth and Planetary Science Letters, 435, 1-13, 10.1016/j.epsl.2015.11.027, 2016.

Koch, P. L., Zachos, J. C., and Gingerich, P.: Correlation between isotope records in marine and continental carbon reservoirs near the Paleocene/Eocene boundary, Nature, 358, 319-322, 1992.

Laskar, J., Robutel, P., Joutel, F., Gastineau, M., Correia, A., and Levrard, B.: A long-term numerical solution for the insolation quantities of the Earth, Astronomy and Astrophysics, 428, 261-285, 10.1051/0004-6361:20041335, 2004.

Littler, K., Röhl, U., Westerhold, T., and Zachos, J. C.: A high-resolution benthic stable-isotope record for the South Atlantic: Implications for orbital-scale changes in Late Paleocene–Early Eocene climate and carbon cycling, Earth and Planetary Science Letters, 401, 18-30, 10.1016/j.epsl.2014.05.054, 2014.

Lourens, L. J., Sluijs, A., Kroon, D., Zachos, J. C., Thomas, E., Röhl, U., Bowles, J., and Raffi, I.: Astronomical pacing of late Palaeocene to early Eocene global warming events, Nature, 435, 1083-1087, 10.1038/nature03814, 2005.

Gelöscht: .

Formatiert: Hervorheben

Gelöscht: Lauretano, V., Littler, K., Polling, M., Zachos, J. C., and Lourens, L. J.: Frequency, magnitude and character of hyperthermal events at the onset of the Early Eocene Climatic Optimum, Clim. Past, 11, 1313-1324, 10.5194/cp-11-1313-2015, 2015. .

Formatiert: Hervorheben

15

Meyers, S. R.: Astrochron: An R Package for Astrochronology, available at: https://CRAN.R-project.org/package=astrochron (last access: 5 September 2017), 2014.

McInerney, F. A., and Wing, S. L.: The Paleocene-Eocene Thermal Maximum: A Perturbation of Carbon Cycle, Climate, and Biosphere with Implications for the Future, Annual Review of Earth and Planetary Sciences, 39, 489-516, doi:10.1146/annurev-earth-040610-133431, 2011.

Murphy, B. H., Farley, K. A., and Zachos, J. C.: An extraterrestrial 3He-based timescale for the Paleocene-Eocene thermal maximum (PETM) from Walvis Ridge, IODP Site 1266, Geochimica et Cosmochimica Acta, 74, 5098-5108, 10.1016/j.gca.2010.03.039, 2010.

Paillard, D., Labeyrie, L., and Yiou, P.: Macintosh program performs time-series analysis., Eos Trans. AGU, 77, (http://www.agu.org/eos_elec/96097e.html), 1996.

Revelle, R., Suess, H.E.: Carbon dioxide exchange between atmosphere and ocean and the question of an increase of atmospheric CO2 during the past decades. Tellus, 9(1): 18-27, 1957.

Röhl, U., Bralower, T. J., Norris, R. D., and Wefer, G.: New chronology for the late Paleocene thermal maximum and its environmental implications, Geology, 28, 927-930, 10.1130/0091-7613(2000)28<927:ncftlp>2.0.co;2, 2000.

Röhl, U., Westerhold, T., Bralower, T. J., and Zachos, J. C.: On the duration of the Paleocene-Eocene thermal maximum (PETM), Geochemistry, Geophysics, Geosystems, 8, 10.1029/2007GC001784, 2007.

Schankler, D.: Faunal zonation of the Willwood Formation in the central Bighorn Basin, Wyoming., in: Early Cenozoic paleontology and stratigraphy of the Bighorn Basin, Wyoming, edited by: Gingerich, P. D., University of Michigan Papers on Paleontology, Ann Arbor, MI, 99-114, 1980.

Sluijs, A., Bowen, G. J., Brinkhuis, H., Lourens, L. J., and Thomas, E.: The Palaeocene–Eocene Thermal Maximumsuper greenhouse: biotic and geochemical signatures, age models and mechanisms of global change, in: Deep-Time Perspectives on Climate Change: Marrying the Signal from Computer Models and Biological Proxies, edited by: Williams, M., Haywood, A. M., Gregory, F. J., and Schmidt, D. N., The Micropalaeontological Society Special Publications, The Geological Society, London, 323-349, 2007.

Sluijs, A., and Dickens, G. R.: Assessing offsets between the $\delta^{13}C$ of sedimentary components and the global exogenic carbon pool across early Paleogene carbon cycle perturbations, Global Biogeochem. Cycles, 26, GB4005, 10.1029/2011gb004224, 2012.

Stap, L., Sluijs, A., Thomas, E., and Lourens, L.: Patterns and magnitude of deep sea carbonate dissolution during Eocene Thermal Maximum 2 and H2, Walvis Ridge, southeastern Atlantic Ocean, Paleoceanography, 24, 10.1029/2008PA001655, 2009.

Thomas, E.: Development of Cenozoic deep-sea benthic foraminiferal faunas in Antarctic waters, in: Origins and Evolution of the Antarctic Biota, edited by: Crame, J. A., Geological Society Special Publication, 283-296, 1989.

Formatiert: Schriftart:Symbol

Formatiert: Hochgestellt

Formatiert: Hervorheben

16

Westerhold, T., Röhl, U., Laskar, J., Bowles, J., Raffi, I., Lourens, L. J., and Zachos, J. C.: On the duration of magnetochrons C24r and C25n and the timing of early Eocene global warming events: Implications from the Ocean Drilling Program Leg 208 Walvis Ridge depth transect, Paleoceanography, 22, 10.1029/2006PA001322, 2007.

5   Westerhold, T., Röhl, U., Raffi, I., Fornaciari, E., Monechi, S., Reale, V., Bowles, J., and Evans, H. F.: Astronomical calibration of the Paleocene time, Palaeogeography, Palaeoclimatology, Palaeoecology, 257, 377-403, 10.1016/j.palaeo.2007.09.016, 2008.

Westerhold, T., Röhl, U., Frederichs, T., Bohaty, S. M., and Zachos, J. C.: Astronomical calibration of the geological timescale: closing the middle Eocene gap, Climate of the Past, 11, 1181–1195,
10   10.5194/cp-11-1181-2015, 2015.

Westerhold, T., Röhl, U., Frederichs, T., Agnini, C., Raffi, I., Zachos, J. C., and Wilkens, R. H.: Astronomical Calibration of the Ypresian Time Scale: Implications for Seafloor Spreading Rates and the Chaotic Behaviour of the Solar System?, Climate of the Past, 13, 1129–1152, 10.5194/cp-13-1129-2017, 2017.

15   Wilkens, R., Westerhold, T., Drury, A. J., Lyle, M., Gorgas, T., and Tian, J.: Revisiting the Ceara Rise, equatorial Atlantic Ocean: isotope stratigraphy of ODP Leg 154, Climate of the Past, 13, 779-793, doi: 10.5194/cp-13-779-2017, 2017.

Zachos, J. C., Röhl, U., Schellenberg, S. A., Sluijs, A., Hodell, D. A., Kelly, D. C., Thomas, E., Nicolo, M., Raffi, I., Lourens, L. J., McCarren, H., and Kroon, D.: Rapid Acidification of the Ocean During
20   the Paleocene-Eocene Thermal Maximum, Science, 308, 1611-1615, 10.1126/science.1109004, 2005.

Zachos, J. C., McCarren, H., Murphy, B., Röhl, U., and Westerhold, T.: Tempo and scale of late Paleocene and early Eocene carbon isotope cycles: Implications for the origin of hyperthermals, Earth and Planetary Science Letters, 299, 242-249, 10.1016/j.epsl.2010.09.004, 2010.

Zeebe, R. E., and Zachos, J. C.: Reversed deep-sea carbonate ion basin gradient during Paleocene-Eocene
25   thermal maximum, Paleoceanography, 22, 10.1029/2006PA001395, 2007.

Zeebe, R. E., Ridgwell, A., and Zachos, J. C.: Anthropogenic carbon release rate unprecedented during the past 66 million years, Nature Geosci, 9, 325-329, 10.1038/ngeo2681, 2016.

Zeebe, R. E., Westerhold, T., Littler, K., and Zachos, J. C.: Orbital forcing of the Paleocene and Eocene carbon cycle, Paleoceanography, 32, 440-465, 10.1002/2016PA003054, 2017.

30

17

Gelöscht: Thomas, E., and Shackelton, N. J.: The Paleocene-Eocene benthic foraminiferal extinctio and stable isotope anomalies, in: Correlationof the Early Paleogene in Northwest Europe, edited by: Knox, R. W. O. B., Corfield, R. M., and Dunay, R. E., Geological Society Special Publication, 401-441, 1996. .

Formatiert: Hervorheben

Gelöscht: Clim. Past Discuss., 11, 1665-1699, 10.5194/cpd-11-1665-2015, 2015

Gelöscht: .
Gelöscht: Discuss.
Gelöscht: 2017, 1-34
Gelöscht: 10.5194/cp-2017-15

Gelöscht: Discussions
Gelöscht: 2017
Gelöscht: 1
Gelöscht: 22
Gelöscht: 10.5194/cp-2016-140

Table 1. **PETM Age Model for Polecat Bench (PCB) and ODP Sites 690, 1262, 1263, 1265, 1266, and 1267.** From left to right: Precession cycle number of the extracted cycles as in Röhl et al. 2007 and this study, the equivalent depth in the Polecat Bench outcrop and the BBCP drill core, the respective depth of the assigned precession cycles in ODP Sites, the relative age to the onset of the PETM assuming 21 kyr duration for each precession cycle counted, and finally the absolute age using 55.930 Ma as the age of the onset of the PETM as in Westerhold et al. 2007.

| Precession cycle No. | | PCB outcrop depth AA08 | PCB mcd this study | Depth | | | | | | Age rel. to onset PETM (Pre=21.0 kyr) | Age PETM @ 55.930 Ma |
Röhl et al., 2007	this study			Site 1262 mcd	Site 1263 rmcd	Site 1265 mcd	Site 1266 mcd	Site 1267 rmcd	Site 690B mbsf		
20	20			135.88	326.56	308.24		227.12	160.42	409	55.521
19	19			136.09	327.01	308.66		227.35	160.98	388	55.542
18	18			136.31	327.53	309.19		227.62	161.57	367	55.563
16+17	17			136.70	328.30	309.85		228.00	162.40	346	55.584
15	16			137.04	329.11	310.44		228.37	163.54	325	55.605
14	15		7.90	137.27	329.58	310.81	302.05	228.70	164.32	304	55.626
13	14		16.10	137.50	330.13	311.29	302.50	228.95	164.87	283	55.647
12	13		23.50	137.75	330.78	311.76	302.95	229.25	165.29	262	55.668
11	12		31.20	138.12	no data	312.31	303.52	229.57		241	55.689
10	11		38.20	138.38	no data	313.01	304.10	229.90	166.24	220	55.710
9	10		44.60	138.73	332.12	313.64	304.70	230.30		199	55.731
8	9		51.00	139.03	332.79	314.21	305.12	230.64	167.20	178	55.752
7	8	56.95	58.20	139.32	333.39	314.66	305.52	230.93		157	55.773
6	7	67.55	65.85	139.53	333.88	315.23	305.93	231.22		136	55.794
5	6	75.45	74.40	139.71	334.29	315.45	306.21	231.40	169.29	115	55.815
4	5	83.35	82.60	139.82	334.57	315.59	306.40	231.52	169.65	94	55.836
3	4	91.90	91.10	139.94	334.82	315.72	306.56	231.63	169.98	73	55.857
2	3	99.95	99.70	140.03	335.04	315.80	306.67	231.69	170.30	52	55.878
1	2	107.85	107.50							31	55.899
missing	1	114.85	115.35							10	55.920
onset PETM			**118.70**	**140.14**	**335.27**	**315.85**	**306.77**	**231.77**	**170.64**	**0**	**55.930**
-1	-1	126.75	123.00	140.23	335.64	316.31	306.92		170.99	-10	55.940
-2	-2		130.00	140.32		316.74	307.20	232.05	171.40	-31	55.961
-3	-3		139.30	140.53				232.27	171.88	-52	55.982
-4	-4		146.50					232.45	172.40	-73	56.003
-5	-5		155.00	140.85	336.86		308.10	232.63	173.14	-94	56.024
-6	-6		164.00	141.04	337.11		308.43	232.85	173.54	-115	56.045
-7	-7		171.20	141.27	337.42		308.80	233.10	173.73	-136	56.066
-8	-8		181.70	141.52	337.82		309.13	233.35	174.11	-157	56.087
-9	-9		189.50	141.74	338.20		309.55	233.65		-178	56.108
-10	-10			141.95	338.47		309.87	233.88		-199	56.129
-11	-11			142.12						-220	56.150
-12	-12		208.70	142.41						-241	56.171
-13	-13			142.63						-262	56.192
-14	-14			142.87					174.34	-283	56.213
-15	-15		228.60	143.10					174.58	-304	56.234
-16	-16		235.70	143.39					174.99	-325	56.255
-17	-17		243.50	143.71						-346	56.276
-18	-18		251.60	143.96					175.65	-367	56.297
-19	-19			144.27					176.05	-388	56.318
-20	-20			144.60					176.45	-409	56.339

Table 2. Age Model for Gilmore Hill (GMH) drill core and regional outcrops. From left to right: Labeling ID for identified precession cycles (see text for details), the respective depth of the assigned precession cycles in the Upper Deer Creek, the Deer Creek and the Gilmore Hill sections as well as the Gilmore Hill BBCP drill core. Precession cycle number as defined in ODP sites counting precession cycles (Westerhold et al. 2007) followed by the relative and absolute age to the onset of the PETM assuming 21 kyr duration for each precession cycle counted, using 55.930 Ma for the onset of the PETM (Westerhold et al. 2007) and using 54.050 Ma for the absolute age of ETM-2 (Westerhold et al. 2017).

ID	Upper Deer Creek meter Abels et al. 2012	Deer Creek meter Abels et al. 2013	Gilmore Hill meter DAmbrosia et al. 2017	GMH mcd	precession cycle no	relative to onset PETM @ 0	Onset PETM @ 55.93 Ma	ETM-2 @54.05 Ma
H2	98.05	-		-	-	-	-	53.950
End of Elmo CIE			920.0		90	1788	54.058	54.008
Elmo	70.00	-	907.0	10.00	88	1830	54.100	54.050
Y	42.29	-	-	26.55	87	1809	54.121	54.071
X	36.30	-	-	33.90	86	1788	54.142	54.092
W	29.63	-	854.5	41.10	85	1767	54.163	54.113
V	23.81	-	-	48.00	84	1746	54.184	54.134
U	-	-	-	54.40	83	1725	54.205	54.155
T	-	-	-	60.40	82	1704	54.226	54.176
S	-	-	824.0	66.80	81	1683	54.247	54.197
R	-	-	-	71.40	80	1662	54.268	54.218
Q	-	-	-	77.20	79	1641	54.289	54.239
P	-	110.9	-	84.80	78	1620	54.310	54.260
O	-	103.8	796.5	92.70	77	1599	54.331	54.281
N	-	96.8	-	98.40	76	1578	54.352	54.302
M	-	-	-	105.60	75	1557	54.373	54.323
L	-	79.5	-	112.70	74	1536	54.394	54.344
K	-	72.6	-	120.70	73	1515	54.415	54.365
J	-	65.8	769.0	127.80	72	1494	54.436	54.386
I	-	59.0	-	134.80	71	1473	54.457	54.407
H	-	52.3	-	141.60	70	1452	54.478	54.428
G	-	46.0	-	153.60	69	1431	54.499	54.449
F	-	-	-	-	68	1410	54.520	54.470
E	-	28.2	-	174.00	67	1389	54.541	54.491
D	-	21.3	-	179.70	66	1368	54.562	54.512
C	-	15.0	-	187.30	65	1347	54.583	54.533
B	-	9.3	-	194.70	64	1326	54.604	54.554
A	-	3.2	-	200.30	63	1305	54.625	54.575
-A	-	-	-	205.90	62	1284	54.646	54.596

19

56.0 Ma Reconstruction
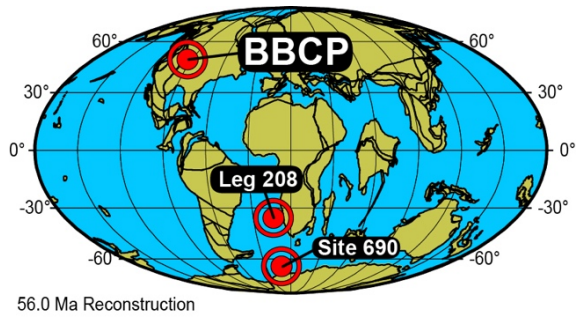
Figure 1: Location map for BBCP (Bighorn Basin Coring Project, Wyoming, USA), ODP Leg 208 (Sites 1260 and 1263) and ODP Leg 113 (Site 690) on a 56 Ma paleogeographic reconstruction in Mollweide projection (from http://www.odsn.de, Hay et al., 1999)

Figure 2: Polecat Bench PCB-A (A) and PCB-B (B) core images, XRF Fe intensity data and spectral analysis on composite depth scale. Core scan images have been assembled with software package IGOR (Wilkens et al. 2017). XRF Fe intensity (black line) with trend (thick red line) that has been removed for following spectral analysis. Residual Fe after trend removal and two Gaussian filters of the dominant cycles 8m (red) and 3.5m (blue). Evolutive spectral plot to decode changes in the cyclicity and thus sedimentation rates. Panels (C) and (D) show the MTM-power spectra for PCB-A and PCB-B Fe data.

Gelöscht:

Gelöscht: subm

21
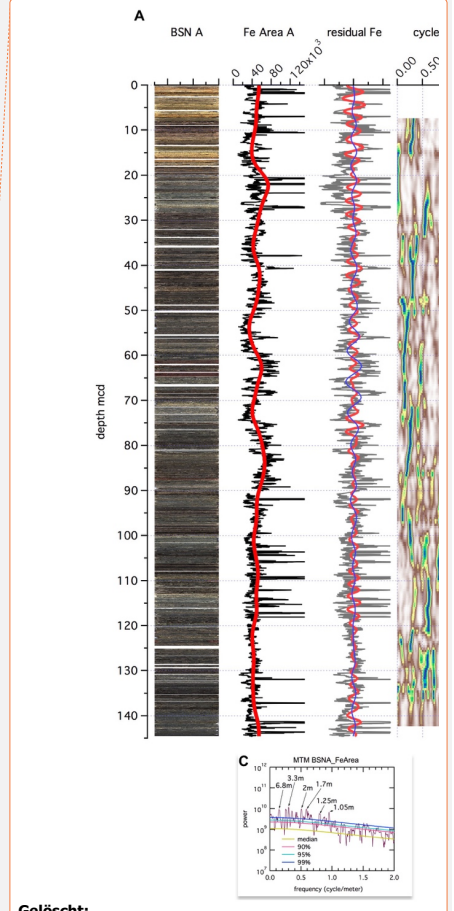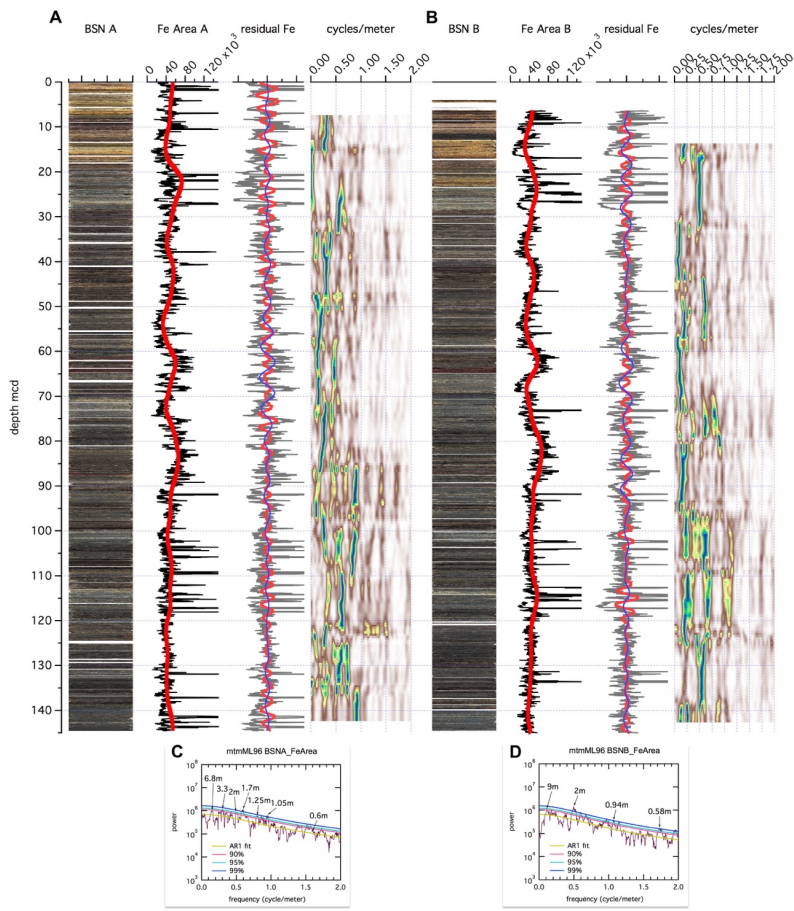
Figure 3: Basin Substation BSN-A (A) and BSN-B (B) core images, XRF Fe intensity data and spectral analysis on composite depth scale. Panels (C) and (D) show the MTM-power spectra for BSN-A and BSN-B Fe data. For details see figure 2.

Gelöscht:

22
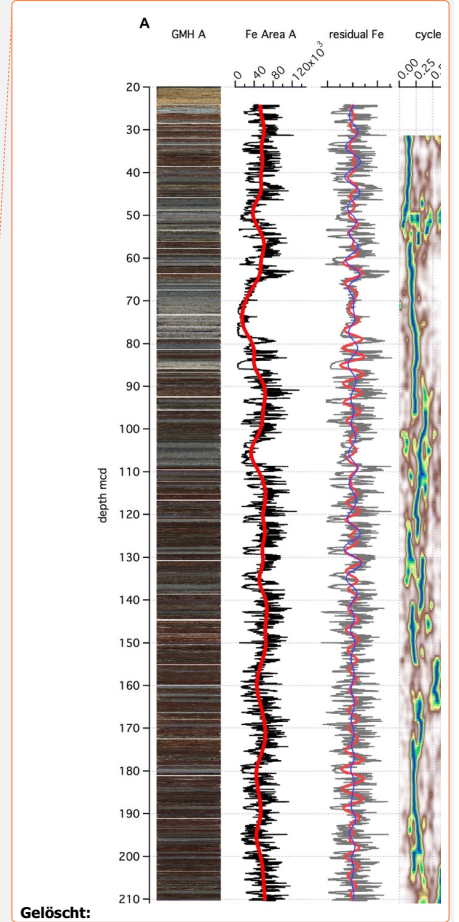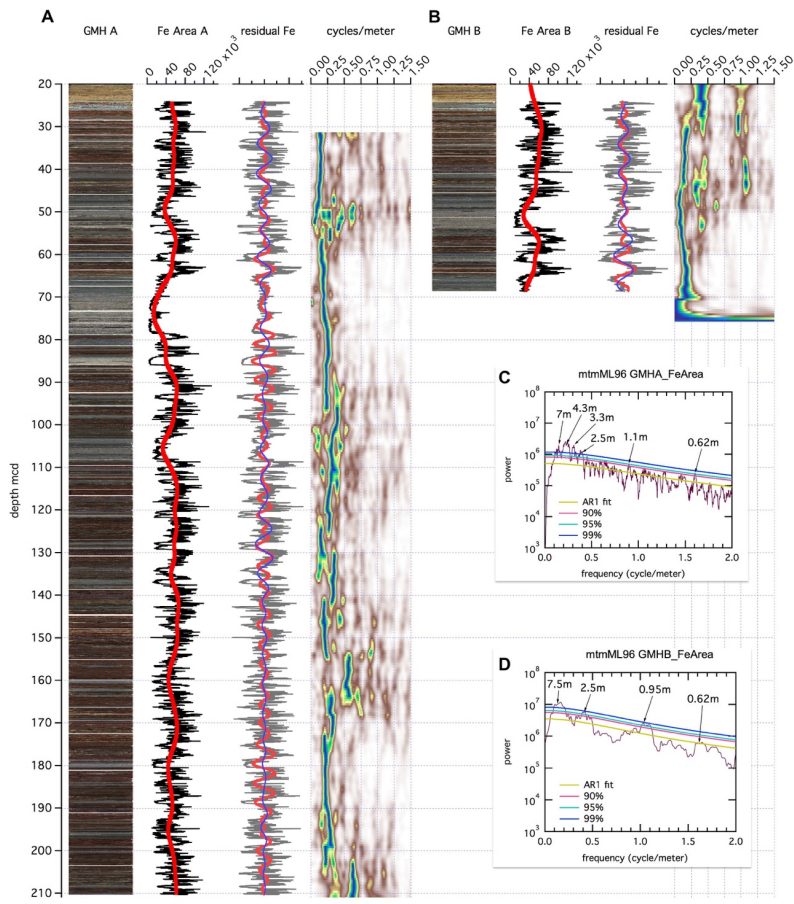
Figure 4: Gilmore Hill GMH-A (A) and GMH-B (B) core images, XRF Fe intensity data and spectral analysis on composite depth scale. Panels (C) and (D) show the MTM-power spectra for GMH-A and GMH-B Fe data. For details see figure 2.

23
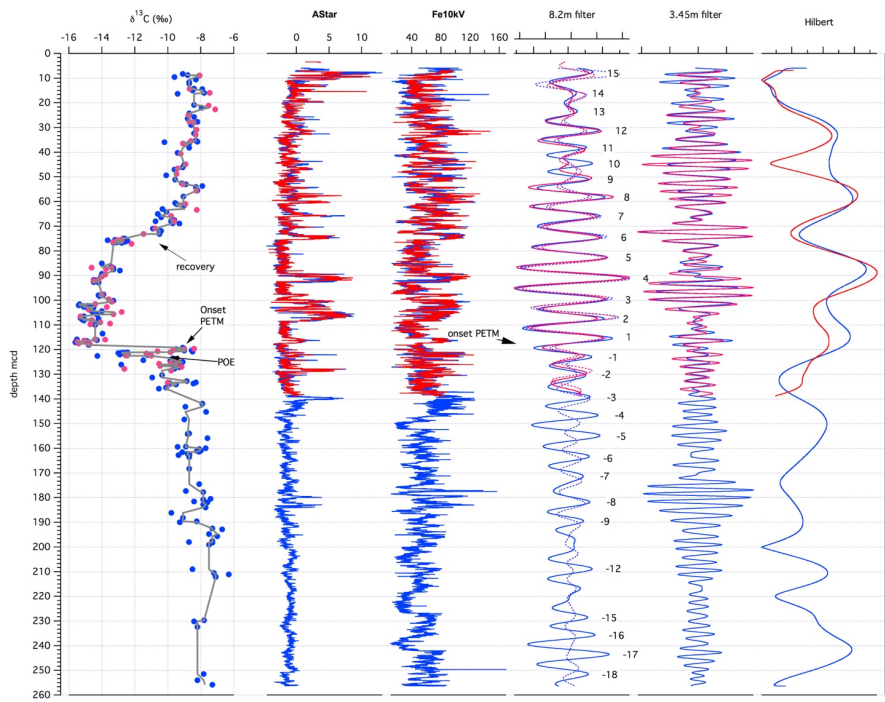
Figure 5: Cyclostratigraphy for Polecat Bench. From left to right: PCB-A(red) and PCB-B (blue) soil nodule carbon isotope data (Bowen et al., 2015), a* data from color scanning, XRF Fe intensity data (in total counts area *1000). Then Gaussian filter of the longer 8.2 m cycle (precession) of the Fe data (solid lines) and from a* data (dashed lines). Numbers mark the precession cycle counting starting at the onset of the PETM, positive numbers is time after PETM, negative numbers before. On the right, Gaussian filter of the 3.5 m cycle (half-precession) and the amplitude modulation of the Fe data extracted by Hilbert transform using the 'Astrochron' software package (Meyers, 2014).
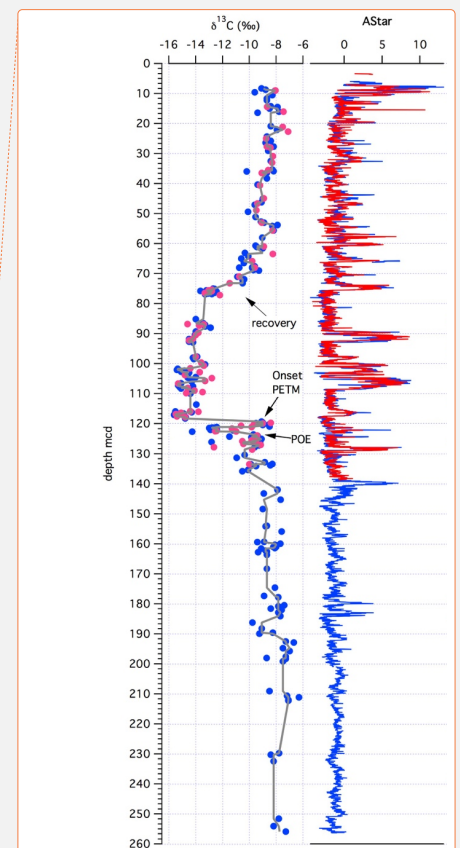
Gelöscht:

Gelöscht: Cyclostratigraphy for Polecat Bench. From left to right: PCB-A(red) and PCB-B (blue) soil nodule carbon isotope data (Bowen et al. 2015), a* data from color scanning, XRF Fe intensity data (in total counts area *1000). Then Gaussian filter of the longer 8.2 m cycle (precession) of the Fe data (lines) and from a* data (dashed lines). Numbers mark the precession cycle counting starting at the PETM, positive numbers is time after PETM, negative numbers before. On the right, Gaussian filter of the 3.5 m cycle (half-precession).

24

Figure 6: Cyclostratigraphy for Gilmore Hill. Left to right: GMH A (red) soil nodule carbon isotope data (Tab. S9) for stratigraphic reference, a* data from color scanning, XRF Fe intensity data (in total counts area *1000). Then Gaussian filter of the longer 7 m cycle (precession) of the Fe data (lines) and from a* data (dashed lines). Letters mark the precession cycle counting following Abels et al. (2013) labeling at Deer Creek Amphitheater. On the right, Gaussian filter of the 4.6 m cycle. Please note: the cyclostratigraphy is straight forward and correlates well to Abels et al. (2013) for the range A to P, however, cycles P to Y are new and not in Abels et al. (2013).

Gelöscht: the

Gelöscht: (half-precession)

25

Figure 7: Overview for the Paleocene-Eocene Thermal Maximum (PETM) data from deep-sea records and the terrestrial Polecat Bench (PCB) drill core against age. Core images and lithology log (Gingerich et al., 2006) for PCB, core images of ODP Sites 1262, 1267, 1266, 1265, 1263 and 690 (aligned from left to right according to the water depth from deep to shallow), defined phases of events in the PETM (Röhl et al., 2007) on the new age model, extracted precession cycles using a Gaussian filter of the PCB XRF Fe intensity data, stable carbon isotope data from PCB soil nodules (Bowen et al., 2015) and the deep sea benthic foraminifera and bulk sediment (690 -Bains et al., 1999; Leg 208 - Zachos et al., 2005), and carbonate content (690 - Farley and Eltgroth, 2003; Leg 208 - Zachos et al., 2005). Letters indicate horizons as identified by Zachos et al., (2005) adjusted to the new age model for the deep-sea sites.

Gelöscht:

Gelöscht: extracted Gaussian filter of the PCB XRF Fe intensity data

26
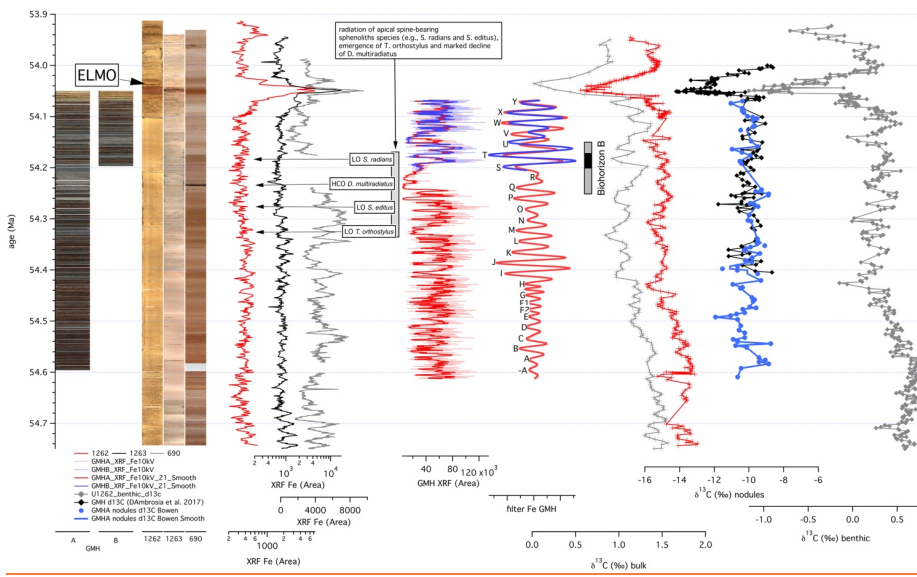
Figure 8: Overview of data for the interval prior to the Eocene Thermal Maximum 2 (ETM-2) from deep-sea records and the terrestrial Gilmore Hill (GMH) drill core against age. Core images for GMH A and B, core images of ODP Sites 1262, 1263 and 690 (aligned from left to right according to the water depth from deep to shallow), XRF Fe core scanning data from 1262 (red), 1263 (black), 690 (grey) (Westerhold et al., 2007), and GMH, extracted Gaussian filter of the GMH XRF Fe intensity data, stable carbon isotope data of soil nodules from the Gilmore Hill area (black – Gilmore Hill section Abels et al., 2012 and D'Ambrosia et al., 2017; blue – GMH drill core) and the deep sea benthic foraminifera (1262 – Littler et al., 2014) and bulk sediment (690 – Cramer et al., 2003; 1262 - Zachos et al., 2010). Position of Biohorizon B is after Abels et al., 2012 and D'Ambrosia et al., 2017 (black bar represents best estimate, gray bars represent conservative estimate – see text for discussion); the change in calcareous nannofossils (gray bar and text box) in ODP Site 1262 from Agnini et al., (2007).

Supplement to

Synchronizing early Eocene deep-sea and continental records – cyclostratigraphic age models for the Bighorn Basin Coring Project drill cores

Thomas Westerhold[1], Ursula Röhl[1], Roy H. Wilkens[2], Phil Gingerich[3], William C. Clyde[4], Scott L. Wing[5], Gabriel J. Bowen[6], Mary J. Kraus[7]

[1]MARUM – University of Bremen, Bremen, 28359, Germany
[2]Hawaii Institute of Geophysics & Planetology, University of Hawaii, Honolulu, HI, 96822, U.S.A.
[3]Museum of Paleontology, University of Michigan, Ann Arbor, Michigan 48109-1079, U.S.A.
[4]Department of Earth Sciences, University of New Hampshire, 56 College Rd., Durham, NH 03824, U.S.A.
[5]Department of Paleobiology, P.O. Box 37012; National Museum of Natural History, Smithsonian Institution, Washington, D.C. 20013 U.S.A.
[6]Department of Geology & Geophysics, University of Utah, Salt Lake City, UT, 84112, U.S.A.
[7]Department of Geological Sciences, University of Colorado at Boulder, UCB 399; Boulder, CO80309, U.S.A.

Gelöscht:

Gelöscht: new

Gelöscht: from

Gelöscht: e

Figure S1: Raw data for Basin Substation (BSN) drill cores. From left to right against depth: Lithology logs for BSN A and B; core scan images; Minolta Color scan LStar, AStar and BStar data (BSN A – red; BSN B – blue); XRF core scanning intensity for Iron Fe (Area) (BSN A – red; BSN B – blue).
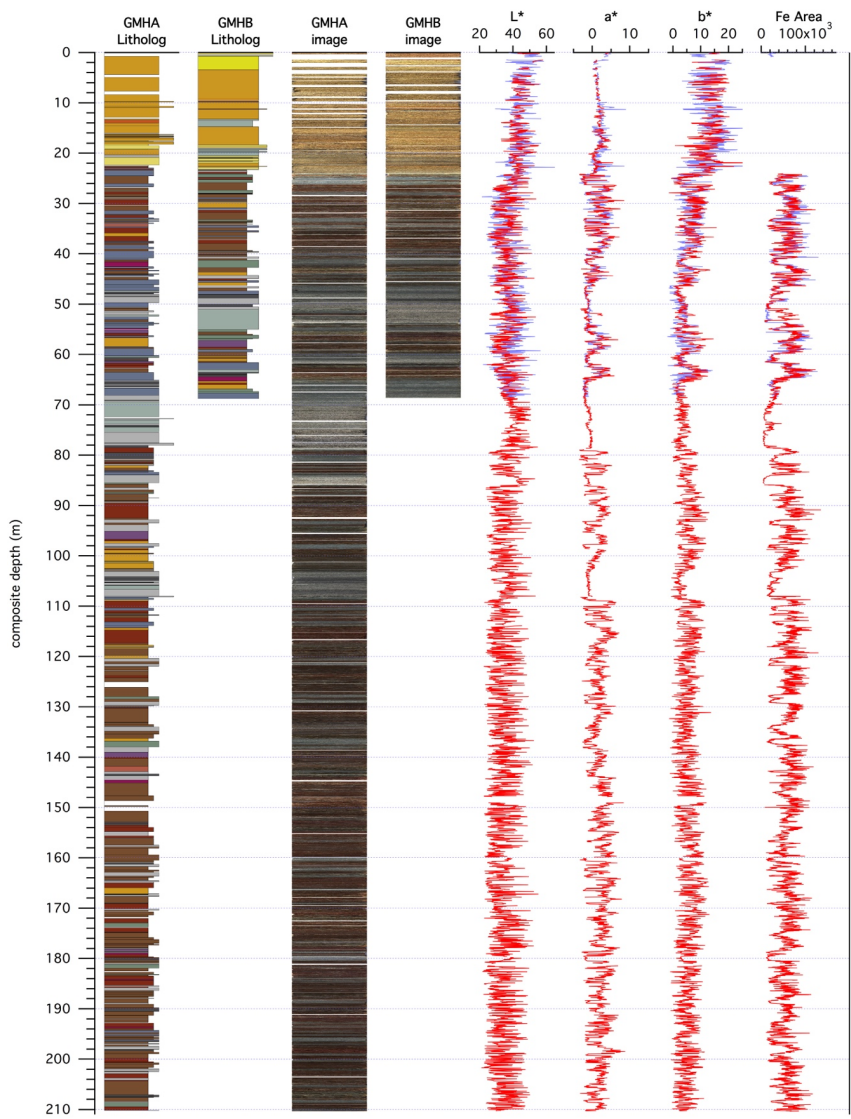
Figure S2: Raw data for Gilmore Hill (GMH) drill cores, for details see figure S1.
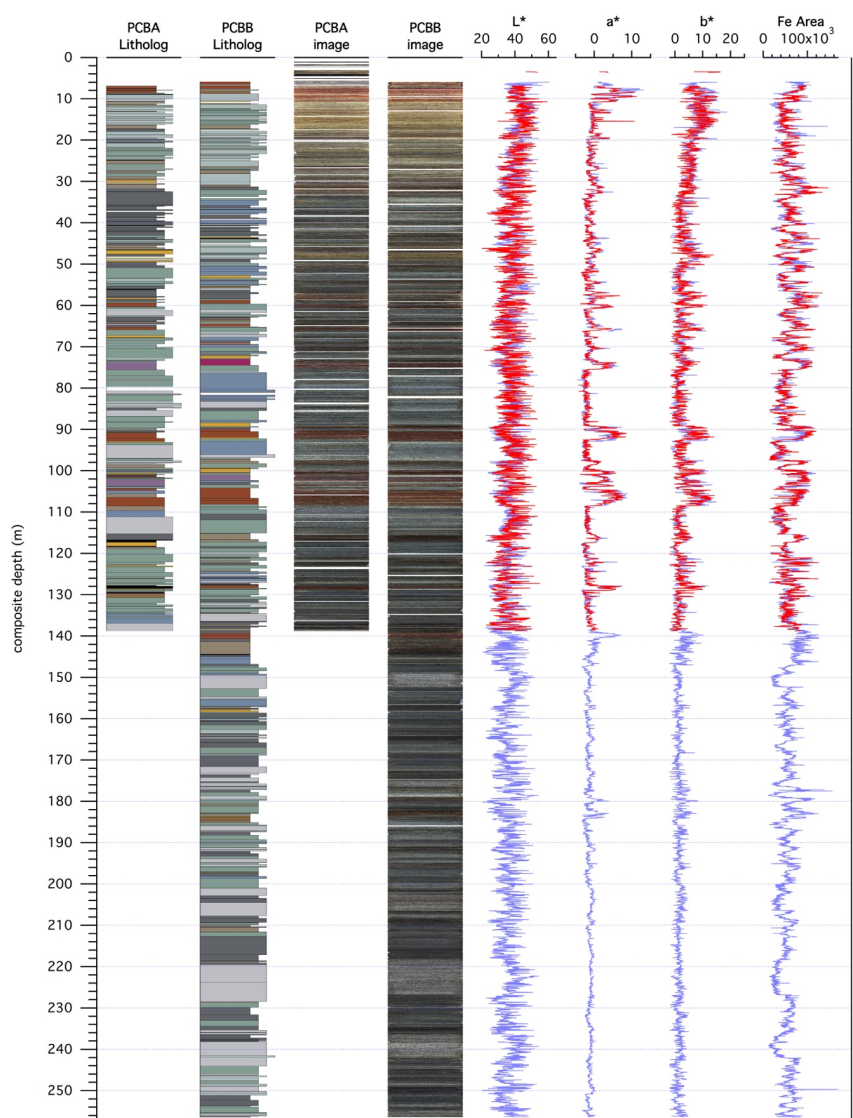
Figure S3: Raw data for Polecat Bench (PCB) drill cores, for details see figure S1.

GMH
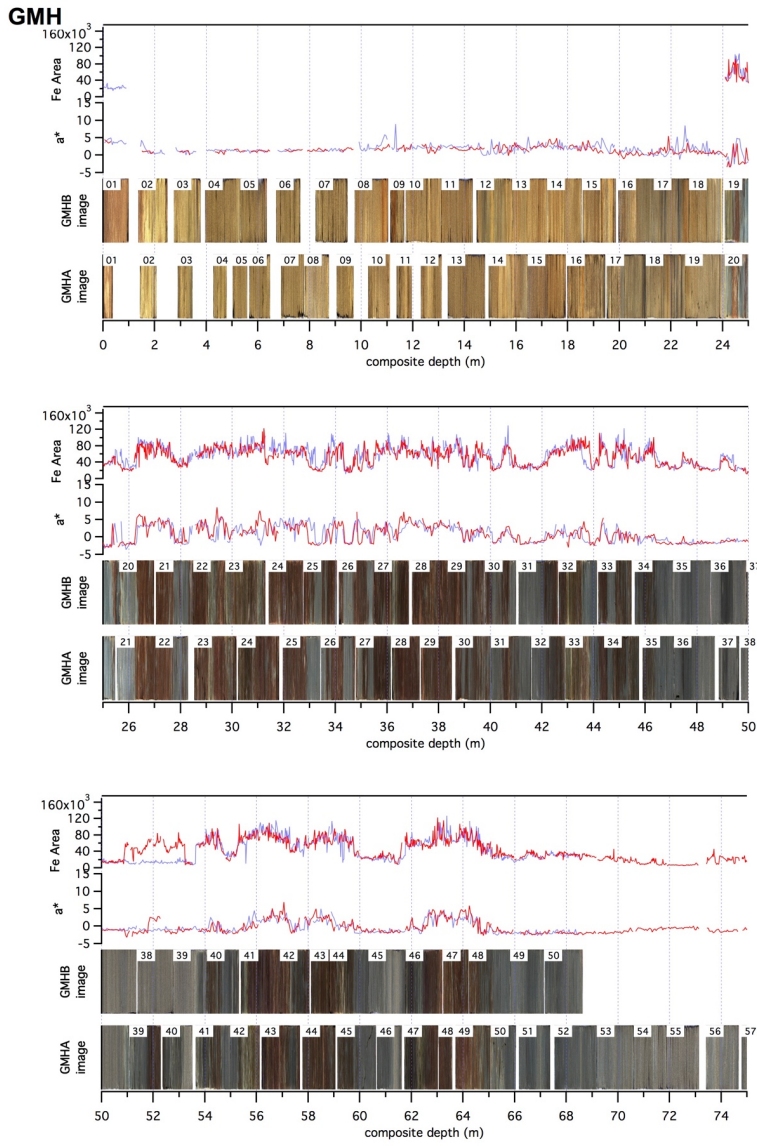
Figure S4: Composite depth plots for GMH. From bottom to top in each panel given are the core image for A and B hole, the a* and XRF Fe intensity data (GMH A – red, GMH B – blue) on composite depth mcd from 0-25, 25-50 and 50-75 mcd. Deeper than 75 mcd there is no parallel hole to correlate to.
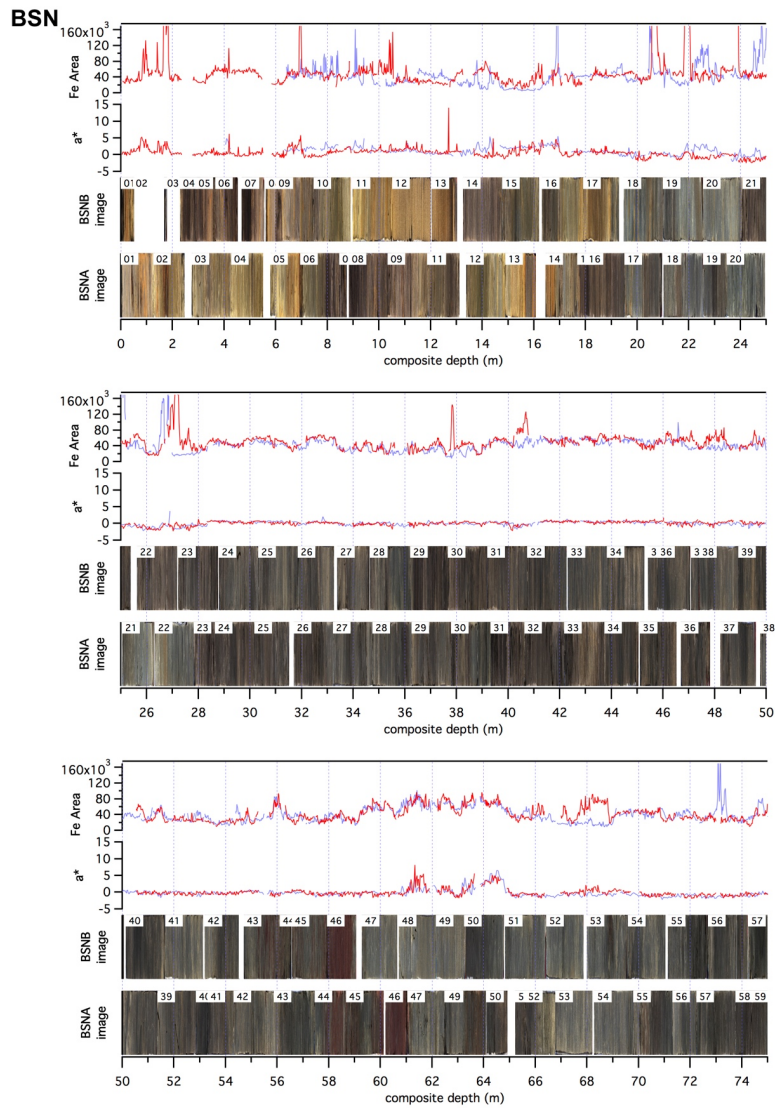
Figure S5a: Composite Depth plots for BSN. For details see figure S4.
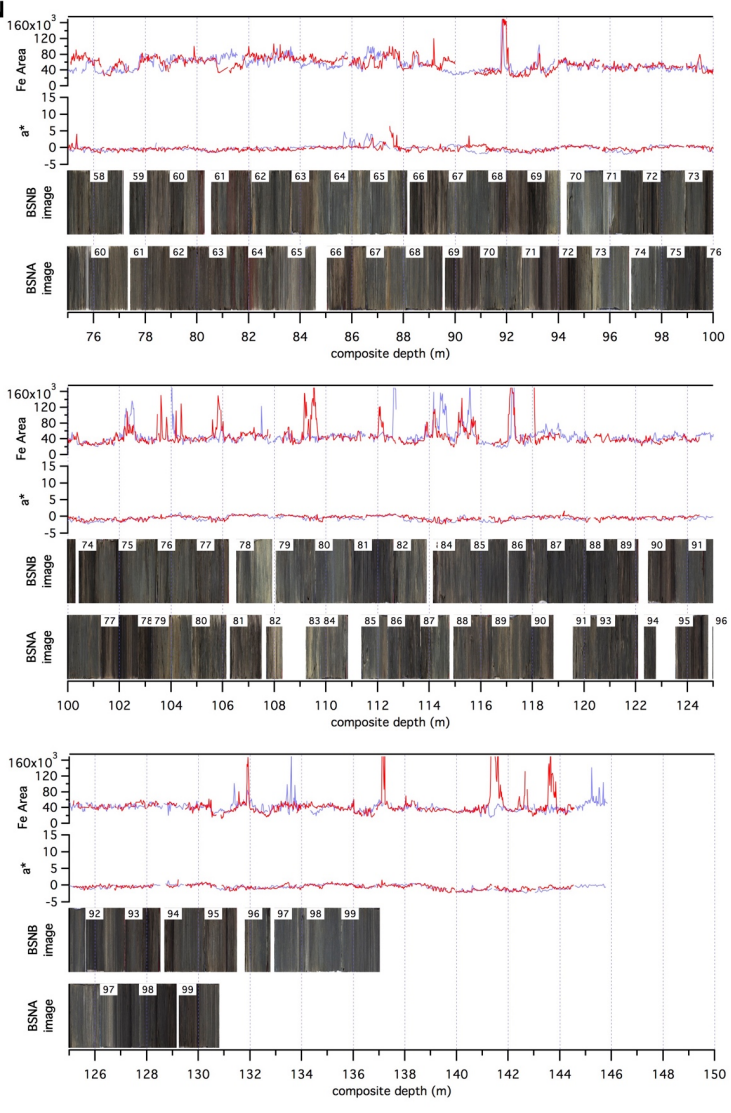
Figure S5b: Composite Depth plots for BSN continued. For details see figure S4.
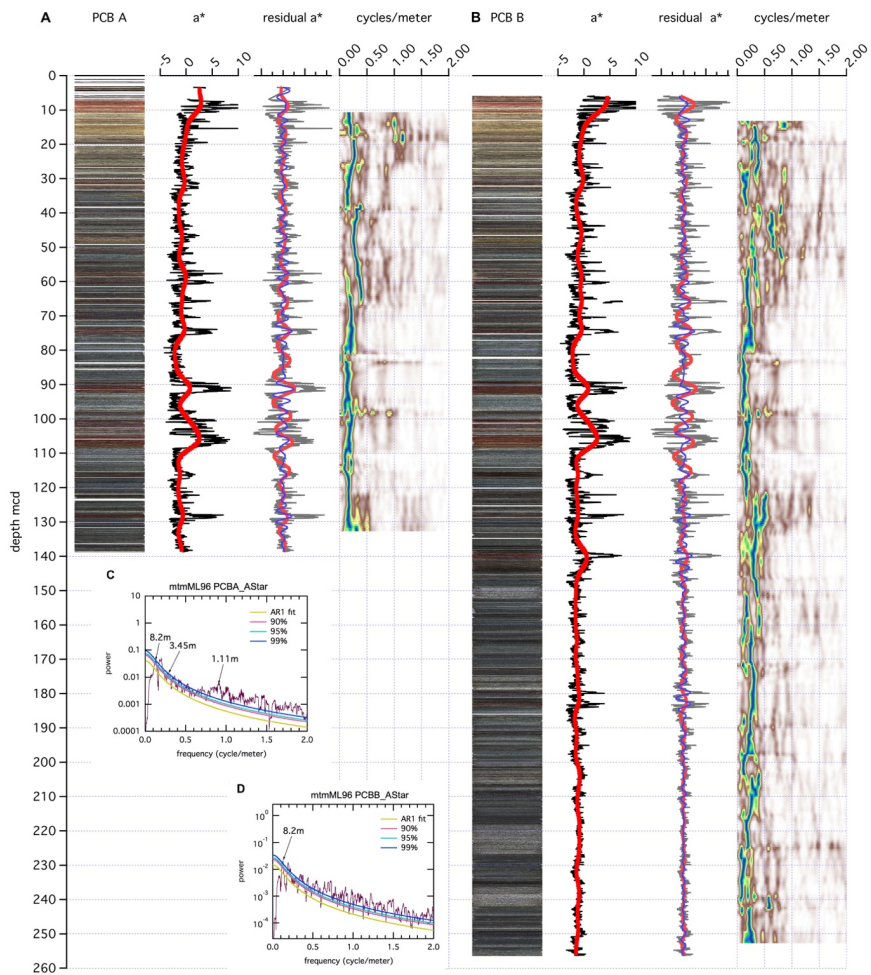
Figure S6: PCB spectral analysis on a* data from PCB A (A) and PCB B (B). Shown here core scan images, a* (black line) with trend (thick red line) that is removed for spectral analysis, the residual a* after trend removal, two Gaussian filters of the dominant cycles (8m, 3.5m), evolutive spectral plot to study changes in cyclicity and sedimentation rates, (C) and (D) figures show the MTM-Power spectra for PCB A and PCB B a*data.
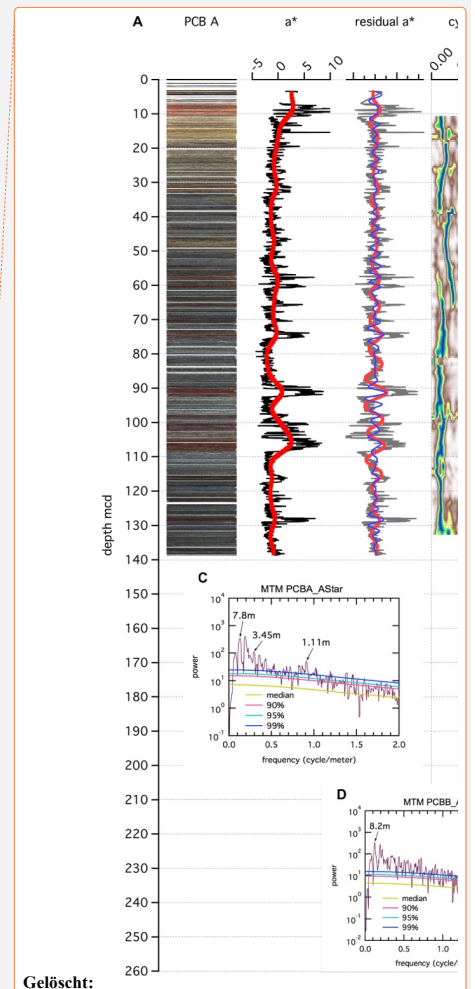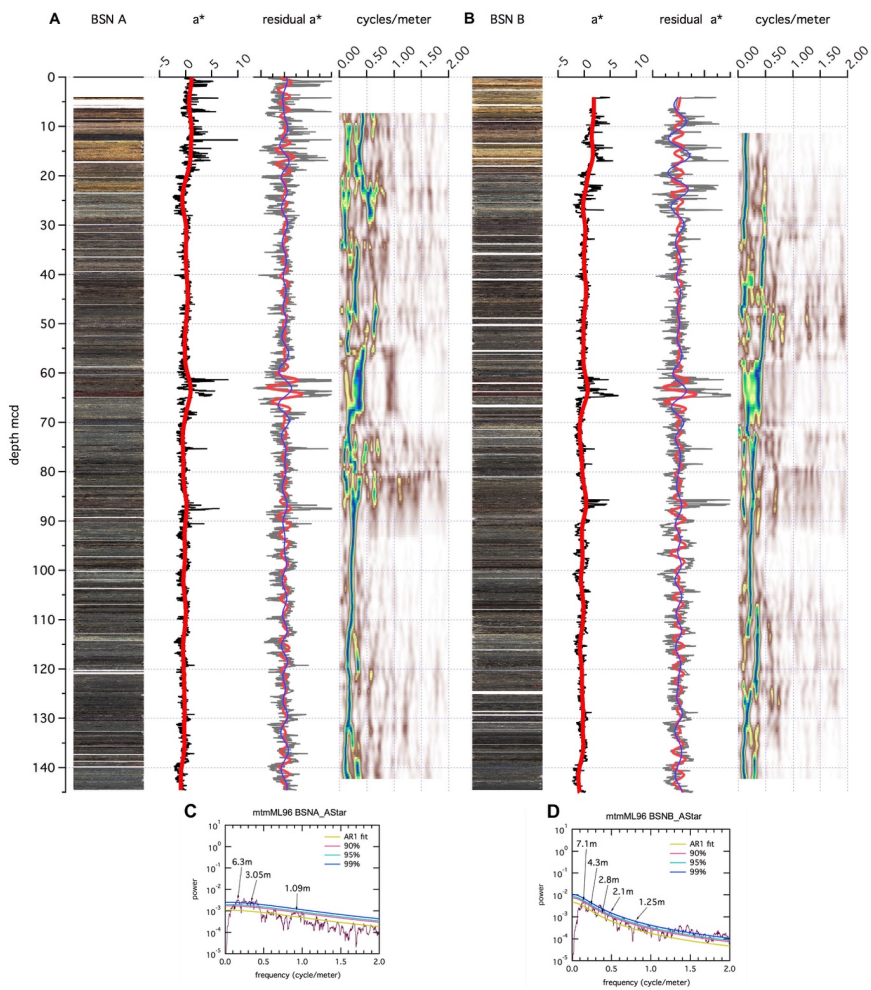
Figure S7: BSN spectral analysis figure for a* data, for details see as figure S6.
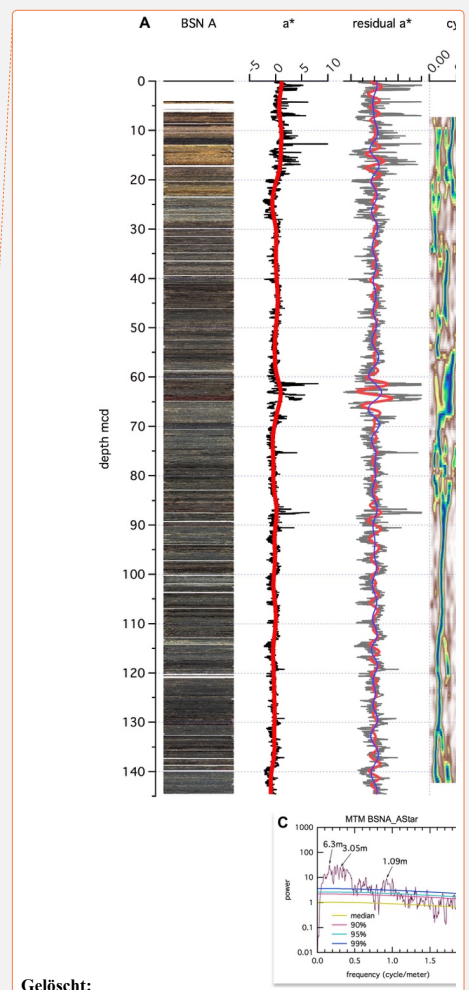
Gelöscht:
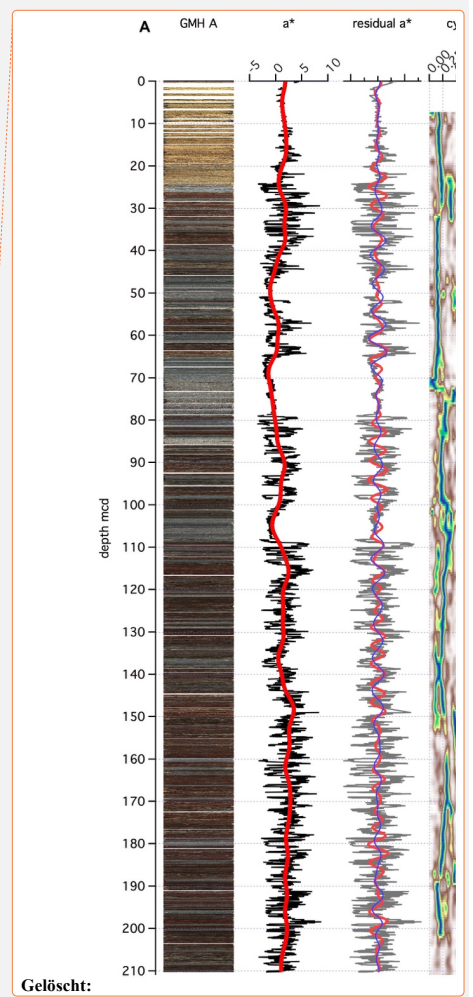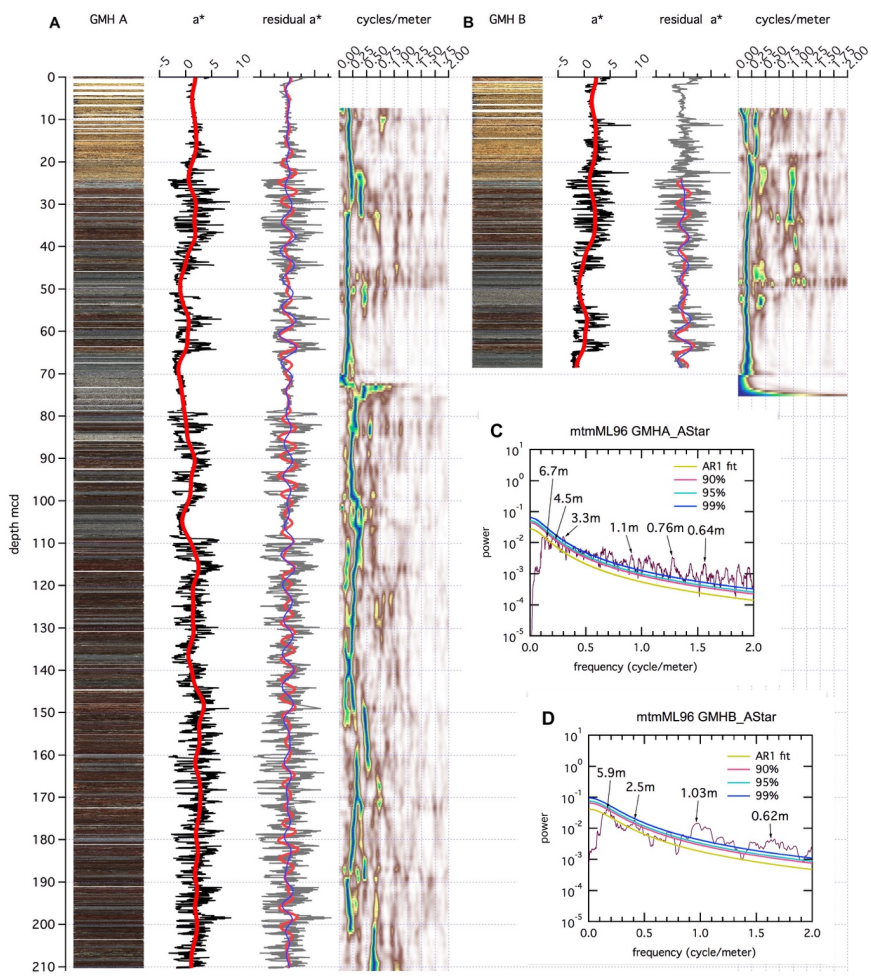
Figure S8: GMH spectral analysis figure for a* data, for details see as figure S6.
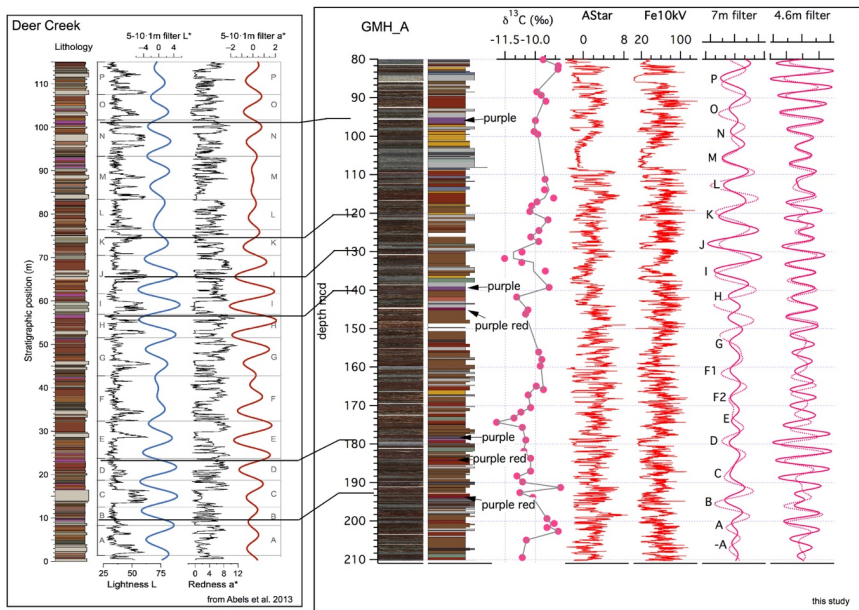
Gelöscht:

Figure S9: GMH correlation to the Deer Creek section (Abels et al. 2013). On the left panel Abels et al. 2013 Deer Creek section lithology with L* and a* data. On the right GMH A images, lithology, δ¹³C data, a*, XRF Fe and filter of cycles with cycle letters. First order correlation was done by the purple beds and the thickness of strata between them. Subsequently the precession cycles were labelled accordingly.
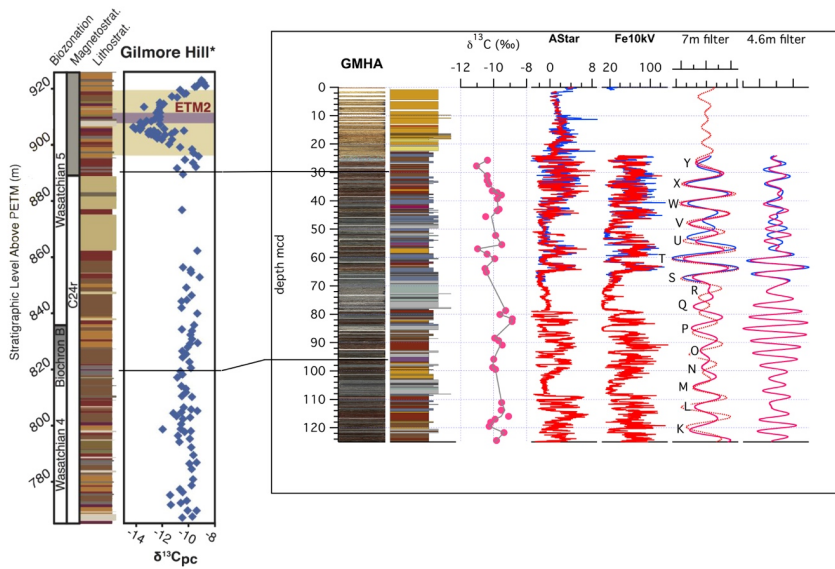
Figure S10: GMH correlation to Gilmore Hill section (DAmbrosia et al., 2017). On the left DAmbrosia et al., 2017 GMH section lithology with δ^{13}C data. On the right GMH A images, lithology, δ^{13}C data, a*, XRF Fe and filter of cycles with cycle letters. First order correlation was done based on field observations. The GMH outcrop and the drillcore have about the same elevation and beds are gently dipping towards the core, thus the ELMO CIE is expected to be in the top 20-30 meters of the core where the sandstone is. Trend toward lower δ^{13}C values right below the sandstone could be the very beginning of the CIE. The purple bed at 96 meters in the GMH core is correlated to the purple bed at 820 m in the outcrop. Precession cycles were labelled accordingly, see main text.

<table>
<tr><td>**Formatiert:** Schriftart:Symbol</td></tr>
<tr><td>**Formatiert:** Hochgestellt</td></tr>
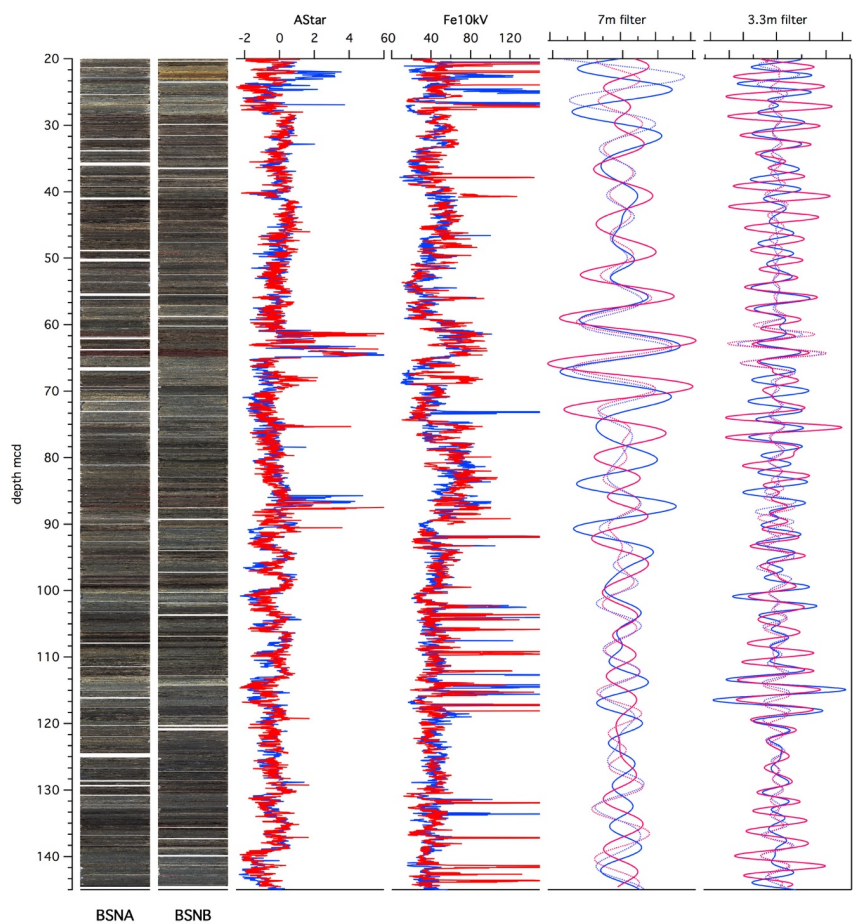<tr><td>**Gelöscht:** d13 C</td></tr>
</table>

Figure S11: Extracted cycles in BSN drill cores. From left to right against depth: BSN A and B core images, a* data, XRF Fe data, Gaussian filter of 7m cycles, Gaussian filter of 3.3m cycles (A – red, B – blue). Note: the precession related 7m cycle does not give consistent results over the entire drill core.
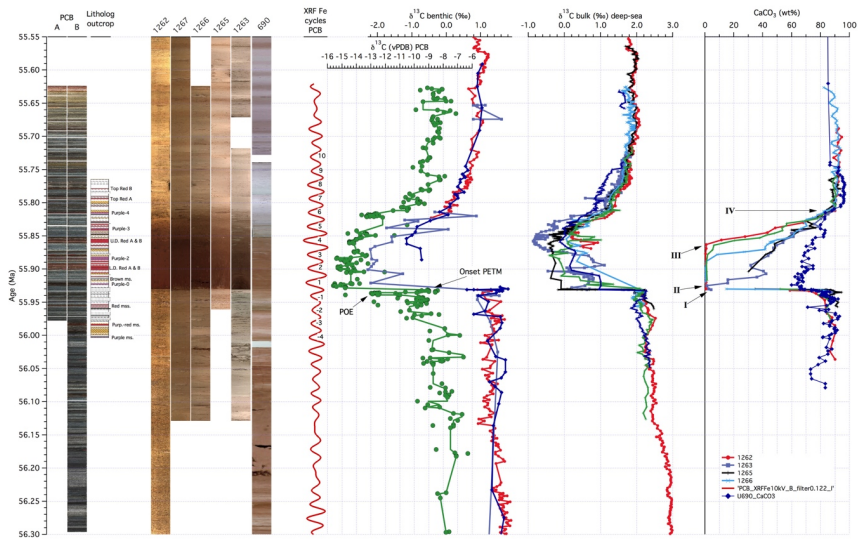
Figure S12: Overview for the Paleocene-Eocene Thermal Maximum (PETM) data from deep-sea records and the terrestrial Polecat Bench (PCB) drill core against age. Core images and lithology log (Gingerich et al., 2006) for PCB, core images of ODP Sites 1262, 1267, 1266, 1265, 1263 and 690 (aligned from left to right according to the water depth from deep to shallow), extracted Gaussian filter of the PCB XRF Fe intensity data, stable carbon isotope data from PCB soil nodules (Bowen et al., 2015) and the deep sea benthic foraminifera and bulk sediment (690 -Bains et al., 1999; Leg 208 - Zachos et al., 2005), and carbonate content (690 – Farley and Eltgroth, 2003; Leg 208 - Zachos et al., 2005). Letters indicate horizons as identified by Zachos et al., (2005) adjusted to the new age model for the deep-sea sites.
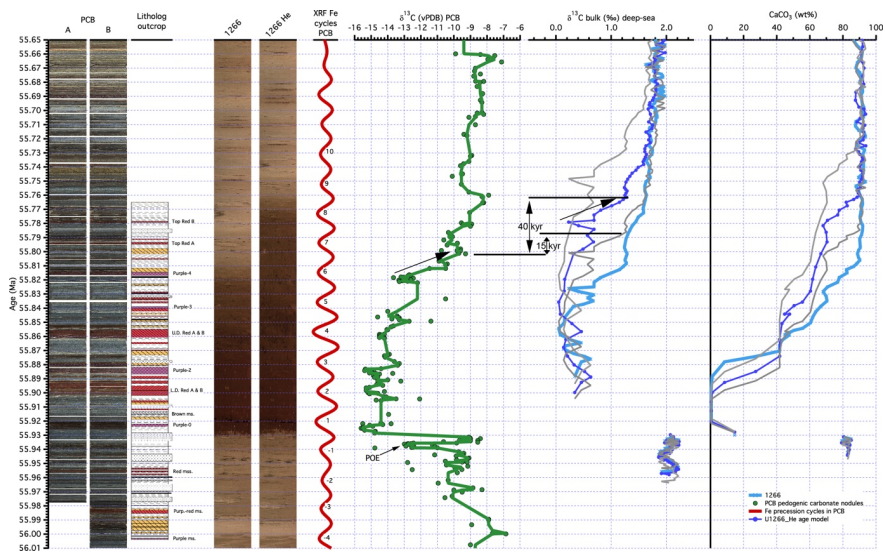
Figure S13: Comparing the updated cyclostratigraphic age model with the extraterrestrial [3]He age model of ODP 1266 (Murphy et al., 2010) for the PETM interval. Core images and lithology log (Gingerich et al., 2006) for PCB, core images of 1266 on cyclostratigraphy and [3]He age model, extracted Gaussian filter of the PCB XRF Fe intensity data, stable carbon isotope data from PCB soil nodules (Bowen et al., 2015), bulk sediment $\delta^{13}C$, and carbonate content data (Zachos et al., 2005) on cyclostratigraphy (light blue) and [3]He age model (dark blue, grey lines mark the upper and lower uncertainty in the age model).